Crb3 is required to organize the apical domain of multiciliated cells

Céline Burcklé, Juliette Raitière, Grégoire Michaux, Laurent Kodjabachian, André Le Bivic

Crb3 is required to organize the apical domain of multiciliated cells

Céline Burcklé[1,*,§], Juliette Raitière[1,‡], Grégoire Michaux[2], Laurent Kodjabachian[3,¶] and André Le Bivic[1,¶]

[1]Aix-Marseille University, CNRS, UMR 7288, Developmental Biology Institute of Marseille (IBDM), Marseille, France
[2]Univ Rennes, CNRS, IGDR (Institut de Génétique et Développement de Rennes), UMR 6290, F-35000 Rennes, France
[3]Aix Marseille University, CNRS, UMR 7288, Developmental Biology Institute of Marseille (IBDM), Turing Centre for Living Systems, Marseille, France

[*]Present address: Univ Rennes, CNRS, IGDR (Institut de Génétique et Développement de Rennes), UMR 6290, F-35000 Rennes, France
[‡]Present address: Charles River Laboratory Saint Nazaire, France
[§]Author for correspondence (celine.burckle@univ-rennes1.fr)
[¶]co-last authors

Abstract

Cell shape changes mainly rely on the remodeling of the actin cytoskeleton. Multiciliated cells (MCCs) of the mucociliary epidermis of *Xenopus laevis* embryos, as they mature, dramatically reshape their apical domain to grow cilia, in coordination with the underlying actin cytoskeleton. Crumbs (Crb) proteins are multifaceted transmembrane apical polarity proteins known to recruit actin linkers and promote apical membrane growth. Here, we identify the homeolog Crb3.L as an important player for centrioles/basal bodies (BB) migration and apical domain morphogenesis in MCCs. Crb3.L is present in cytoplasmic vesicles close to the ascending centrioles/BBs where it partially colocalizes with Rab11a. Crb3.L morpholino-mediated depletion in MCCs caused abnormal migration of centrioles/BBs, reduction of their apical surface, disorganization of their apical actin meshwork, and defective ciliogenesis. Rab11a morpholino-mediated depletion phenocopied Crb3.L loss-of-function in MCCs. Thus, the control of centrioles/BBs migration by Crb3.L might be mediated by Rab11a-dependent apical trafficking. Furthermore, we show that both phospho-activated ERM (pERM) and Crb3.L are recruited to the growing apical domain of MCCs, where Crb3.L likely anchors pERM allowing actin-dependent expansion of the apical membrane.

Key words: Crumbs; ERM; Rab11a; multiciliated cells; apical actin cytoskeleton; *Xenopus*

Introduction

Epithelia are lining the external surface and body cavities in animals and ensure exchanges with the extracellular environment as well as protection of internal organs (Buckley and St Johnston,

2022; Rodriguez-Boulan and Macara, 2014). This dual function relies on the organization of epithelial sheets. Epithelial cells are highly polarized, exhibiting structurally and functionally distinct apical and basolateral domains (Román-Fernández and Bryant, 2016). In a majority of epithelia in vertebrates, the apical surface forms microtubule-based protrusions called cilia (Apodaca, 2018). Primary cilia are antenna-like organelles perceiving a variety of environmental cues, including crucial signaling morphogens (Anvarian et al., 2019; Bangs and Anderson, 2017). In the ciliated epithelia lining the airways, the brain ventricles, or the reproductive tracts, the apical domain of multiciliated cells (MCCs) is covered by numerous cilia beating coordinately to propel biological fluids (Boutin and Kodjabachian, 2019; Spassky and Meunier, 2017). Thus, structural and/or functional alteration of cilia lead to rare diseases with pleiotropic symptoms called ciliopathies (Reiter and Leroux, 2017).

Xenopus is a powerful model for studying motile cilia biology (Walentek, 2021; Werner and Mitchell, 2012). The embryos are indeed enwrapped in a protective mucociliary epidermis composed of MCCs, bearing hundreds of motile cilia, alternating in a salt and pepper pattern with secretory cell types (goblet cells, ionocytes and small secretory cells (SSCs)) (Boutin and Kodjabachian, 2019; Walentek, 2021). The development of the *Xenopus* epidermis is a gradual process starting at segmentation/blastula stages with the partitioning of the prospective non-neural ectoderm into an outer epithelial layer made of goblet cells, and an inner mesenchymal layer where MCCs, ionocytes, SSCs and p63+ basal cells will be born (Deblandre et al., 1999; Dubaissi et al., 2014; Dubaissi and Papalopulu, 2011; Haas et al., 2019; Quigley et al., 2011; Stubb et al., 2006; Walentek et al., 2014). From mid-neurula onwards (Stages 14-31), intense morphogenetic events reshape the tissue, with the sequential insertion of MCCs, ionocytes and SSCs in the outer layer, where they complete differentiation (Haas et al., 2019). Successful intercalation of MCCs is powered by cell shape changes and forces generated by the actin and microtubule cytoskeletons (Boisvieux-Ulrich et al., 1987; Chuyen et al., 2021; Collins et al., 2021, 2020; Lemullois et al., 1988; Sedzinski et al., 2016; Werner et al., 2011). Prior to their intercalation, MCCs undergo random planar migration, constrained by homotypic repulsion, such that they eventually disperse and intercalate at regular intervals (Chuyen et al., 2021). MCC movement is confined to the grooves formed between overlying epithelial cells (Chuyen et al 2021). Radial intercalation involves the emission by MCCs of filopodia that pull on outer-layer junctions to probe their stiffness (Ventura et al., 2022). MCCs preferentially intercalate into stiff high fold vertices, where they provoke remodeling of the junction in preparation for apical expansion (Ventura et al., 2022). Once inserted into the outer layer, MCCs expand their apical domain, essentially via the 2D pressure exerted by a highly dynamic medial actin network generated by Formin 1 (Sedzinski et al., 2017, 2016).

While inserting into the outer layer, MCCs multiply centrioles deep in the cytoplasm, which are then encased via CP 110 and the ciliary adhesion complex (FAK, Paxillin, Vincullin, Talin) in an internal actin network that drives their apical migration (Antoniades et al., 2014; Walentek et al., 2016). Once docked at the apical surface, centrioles are named basal bodies (BBs). The dynamic ascension of centrioles relies on actomyosin contractility and is regulated by actors of the PCP signaling pathway, the core protein Dishevelled, the ciliogenesis and planar polarity effector (CPLANE) protein Inturned and the PCP effector RhoA (Adler and Wallingford, 2017; Boisvieux-Ulrich et al., 1990; Park et al., 2008, 2006). BBs serve as scaffold to initiate ciliogenesis, and are equipped with a basal foot and striated rootlets, which interact with actin filaments and microtubules to establish a regular lattice able to sustain intense ciliary beating strokes (Herawati et al., 2016; Mahuzier et al., 2018; Spassky and Meunier, 2017; Werner et al., 2011). In particular, an extensive reconstruction of the cortical actin meshwork in two layers enables the planar polarized anchoring of BBs to permit directional beating (Boisvieux-Ulrich et al., 1990; Ioannou et al., 2013; Mahuzier et al., 2018; Mitchell et al., 2007; Park et al., 2008, 2006; Werner et al., 2011). At stage 25, the most apical actin layer reaches its final density, actin bundles progressively encircle each BB, and from stage 26 onwards eventually mature in actin-based protrusion called microridges (Werner et al., 2011; Yasunaga et al., 2022). At stage 29-30, the definitive sub-apical actin layer connects each BB to its immediate posterior neighbour via ciliary adhesion complexes and to microridges via Ezrin (Antoniades et al., 2014; Werner et al., 2011; Yasunaga et al., 2022). This sophisticated actin architecture allows coordinated cilia beating, thus ensuring efficient flow production to clear the surface of the embryo from surrounding microbes (Dubaissi et al., 2018; Nommick et al., 2022).

To allow cell shape changes, deformation of the actin cytocortex must be coupled to deformation of the plasma membrane (Clark et al., 2014). The plasma membrane is attached to the underlying cytoskeleton via specific regulated linker proteins such as the ERM protein Ezrin (Clark et al., 2014; Pelaseyed and Bretscher, 2018). In *Xenopus* MCCs, overexpressed versions of Ezrin have been shown to accumulate in the newly expanding apical membrane of intercalating cells, and from there to be superimposed on the apical actin meshwork maturing into microridges (Yasunaga et al., 2022). Ezrin depletion in *Xenopus* MCCs induces a functional alteration of the actin cytoskeleton, impacting centriole/BB migration, apical microridge formation, and anchoring of BBs to microridges (Epting et al., 2015; Yasunaga et al., 2022). Thus, the fine-tuned localization of Ezrin correlates with the control of MCC terminal differentiation. However, the molecular mechanisms underlying the proper control of Ezrin subcellular localization in *Xenopus* MCCs are elusive.

The Crumbs (Crb) polarity proteins have pivotal functions in processes involving quick remodeling of the actin cytoskeleton in coordination with the adjacent membrane and are ERM biochemical and genetical interactors (Aguilar-Aragon et al., 2020; Bajur et al., 2019; Flores-Benitez and Knust, 2015; Gao et al., 2016; Kerman et al., 2008; Letizia et al., 2011; Médina et al., 2002; Salis et al., 2017a; Schottenfeld-Roames et al., 2014; Sherrard and Fehon, 2015; Simões et al., 2022; Tilston-Lünel et al., 2016; Vernale et al., 2021; Wei et al., 2015; Whiteman et al., 2014a). Biochemical studies have demonstrated that the Crb cytoplasmic tail possesses a FERM (Four-point one, ezrin, radixin, moesin) domain allowing ERM binding (Médina et al., 2002; Sherrard and Fehon, 2015; Tilston-Lünel et al., 2016; Wei et al., 2015; Whiteman et al., 2014a). Functional studies essentially performed in *Drosophila* embryos showed that Crb stabilizes the ERM protein Moesin at specific sub-apical domains depending on the nature of the remodeling tissues (Letizia et al., 2011; Salis et al., 2017a; Sherrard and Fehon, 2015). Crb and ERM both independently organize the apical cytocortex and interact genetically for dampening the actomyosin contractility during dorsal closure in *Drosophila* embryos (Bazellières et al., 2018; Fehon et al., 2010; Flores-Benitez and Knust, 2015). In vertebrates, the Crumbs family member Crb3 displays a quasi-ubiquitous epithelial expression (Bazellieres et al., 2009). Strikingly, Crb3- and Ezrin-deficient mice display the same abnormal intestinal phenotype, with villi fusion and microvilli atrophy (Charrier et al., 2015a; Saotome et al., 2004; Whiteman et al., 2014a). Both Ezrin and Crb3 have been shown to be required for ciliogenesis (Bazellières et al., 2018; Bo et al., 2023; Epting et al., 2015; Fan et al., 2007, 2004a; Hazime and Malicki, 2017).

The small Rab-GTPase Rab11 is a central regulator of both apical trafficking and ciliogenesis as it initiates a Rab-GTPase cascade driving membrane delivery for primary cilia growth (Knödler et al., 2010). In several model systems, Crb colocalizes with Rab11 endosomes that are required for Crb apical delivery (Aguilar-Aragon et al., 2020; Bo et al., 2023; Buck et al., 2023; Iioka et al., 2019; Schlüter et al., 2009). In addition, Rab11 is expressed in Xenopus MCCs accumulating in their subapical domain at the time of their intercalation (Kim et al., 2012), and Rab11 depleted MCCs displayed reduced apical surface.

We therefore investigated how Crb3, ERM and Rab11 could cooperate to organize the apical domain and build protrusions, such as cilia in Xenopus MCC.

Results

Crb3.S and Crb3.L display distinct and dynamic expression pattern in the mucociliary epidermis of *Xenopus laevis* embryos.

In *Xenopus laevis*, there are two *crb3* homeologs, *crb3.S* and *crb3.L*, with highly conserved DNA (85 % identity) and protein (85 % identity) sequences. As no tools were available to observe the precise endogenous localization of Crb3 proteins in *Xenopus laevis*, custom-made homeolog specific antibodies were generated. To do so, we chose the extracellular domain of Crb3.S (QNVTTPAPGKLSESA) and Crb3.L (QNVTTSAPDRLSESAR) as immunogens, as this region is the most divergent between the two proteins (non-identical amino acids are underlined). To assess the specificity of the Crb3.L and Crb3.S antibodies, we performed competition assays with the corresponding immunogenic peptides, which caused the extinction of immunofluorescent (IF) signals in whole-embryos (supplementary figures 2A, 2B and 3). By combining these new tools with Utrophin labelling that stains the actin meshwork, acetylated-Tubulin that stains stable cytoplasmic microtubules and cilia, and Centrin that stain centrioles and BBs, we were able to show that Crb3.L and Crb3.S have dynamic and exclusive patterns in the mucociliary epidermis of *Xenopus* embryos (figure 1 and supplementary figure 1).

We focused on the expression of Crb3.L in intercalating MCCs (figure 1). As Crb are transmembrane proteins, punctuate cytoplasmic staining likely corresponds to vesicles. In inserting MCCs, Crb3.L-positive vesicles start to accumulate deep in the cytoplasm close to microtubule arrays (figure 1 A, A1), at the level of the internal actin meshwork (figure 1 B, B'), in the vicinity the ascending centrioles (figure 1 C,D). Next, as apical emergence and conjoint centriole ascension proceeds, Crb3.L is progressively redistributed to the expanding apical domain proximate to actin filaments (figure 1, B, B', C, D) and appears in the ciliary shaft of growing cilia (figure 1, A2). In contrast, Crb3.S exhibits an earlier and wider expression, being detected in all cells of the outer layer during gastrulation (supplementary figure 1). From gastrulation onwards, Crb3.S expression level is prominent in goblet cells, albeit at variable levels, presumably absent from ionocytes and particularly high in SSCs (supplementary figure 1, supplementary figure 3). Strikingly, it is very low or absent from intercalating and mature MCCs (supplementary figure 1, supplementary figure 3).

Based on this analysis and the central function of Crb proteins in cell shape changes empowered by quick actin remodeling, we decided to evaluate the role of Crb3.L in the morphogenesis of the apical domain of MCCs.

Crb3.L is required for proper ciliogenesis

To address the function of *crb3.L* during ciliogenesis, we used an antisense morpholino knockdown strategy with two morpholinos targeting either the translation initiation site (*ATG-crb3.L-*

mo) or the 5'untranslated region (*5'UTR-crb3.L-mo*) of the *crb3.L* mRNA. The efficiency of *5'UTR-crb3.L-mo* was evidenced by the extinction of Crb.3L IF staining in whole-embryos, in both MCCs and non-MCCs (supplementary figure 2B). To unravel a potential effect on ciliogenesis, we examined stage 28 embryos, when MCCs are mature, with a well-developed ciliary tuft (Figure 2, control). Crb3.L depletion affected the aspect of the ciliary tuft of MCCs, which contained fewer cilia. Quantitative analysis revealed that ciliogenesis was significantly impaired upon injection of either of the *crb3.L* targeting morpholinos, with 30% (confidence interval 24-37%, *ATG-crb3L-mo*) to 39 % (confidence interval 26-53%, *5'UTR-crb3.L-mo*) of morphant MCCs forming abnormal ciliary tufts with a strong reduction in the number of cilia (figure 2). As the two *crb3.L* targeting morpholinos displayed comparable effects, *5'UTR-crb3.L-mo* was used in the rest of the study.

Crb3.L is required for proper apical positioning of BBs

As correct BBs apical docking is a prerequisite for proper ciliogenesis, we compared BBs position in tracer-injected control and morphant MCCs. Two complementary approaches were used to observe the organization of BBs: immunolabelling and transmission electron microscopy (TEM). At stage 28, in the control situation, BBs cover most of the apical area, with quite a regular distribution (figure 3, A, B, E, F, I). In contrast, in *5'UTR-crb3L-mo*-injected MCCs, defaults in BBs position and distribution are readily apparent in confocal and TEM images. BBs remained stuck into the cytoplasm (figure 3 C, D, G, H, I) or unevenly scattered, forming clumps when they reached the apical surface (figure 3 I). To quantify the penetrance of this phenotype, we analyzed two parameters: the number of BBs reaching the apical domain and the dispersion of BBs along the apico-basal axis (figure 3 J, K). The number of BBs reaching the apical surface was drastically decreased in morphant compared to control MCCs (figure 3 J). Furthermore, BBs were located significantly deeper into the cytoplasm of morphant compared to control MCCs (figure 3 K). Importantly, both aspects of the BB phenotype were significantly rescued by the injection of a *HA*-tagged *Crb3.L* construction insensitive to the *5'UTR-crb3.L* morpholino (figure 3 J, K).

All these data demonstrated that Crb3.L is essential for an efficient apical migration and/or docking of centrioles/BBs.

Crb3.L is required for proper cortical actin meshwork organization in mature MCCs

Migration/docking of BBs is a stepwise process relying on proper actin meshwork dynamics and organization. In several models, Crb has been shown to regulate actin dynamics (Bazellieres et al., 2009; Flores-Benitez and Knust, 2015; Röper, 2012; Salis et al., 2017b; Sherrard and Fehon, 2015; Simões et al., 2022). As Crb3.L-positive vesicles are detected at the time the actin meshwork remodels (Figure 1) (Ioannou et al., 2013), we hypothesized that Crb3.L could be involved actin

cytoskeleton organization in MCCs. We therefore assessed apical actin meshwork organization in stage 28 control and *5'UTR-crb3L-mo*-injected MCCs. In both noninjected (yellow contour arrowheads) and injected (white contour arrowheads) control cells, the labeled actin meshwork was dense, structured, and actin meshwork found in close proximity to the cell-cell junctions (figure 4 A, B, I, J). In *5'UTR-crb3L-mo*-injected MCCs (c), the central actin meshwork appeared much dimer, fragmented and largely disconnected from the cell junctions (figure 4, E, F, K, L). Measurement of apical medial actin staining intensity confirmed a drastic decrease of about 40 % in morphant compared to control MCCs (figure 4 N). At this stage, the mean apical medial area of MCCs was not significantly different between the two groups, suggesting that in mature MCCs there is no strict correlation between the apical cell surface area and the actin meshwork density (figure 4M).

These results show that in mature MCCs, Crb3.L is required for proper organization of the cortical actin meshwork, but seems dispensable for the expansion of the apical domain to its final dimension.

Endogenous pERM associates dynamically with ascending centrioles/BBs and the apical actin meshwork

We and others have shown that ERM and CRB proteins cooperate for apical domain construction (Aguilar-Aragon et al., 2020; Bajur et al., 2019; Flores-Benitez and Knust, 2015; Letizia et al., 2011; Médina et al., 2002; Salis et al., 2017a; Sherrard and Fehon, 2015; Tilston-Lünel et al., 2016; Wei et al., 2015; Whiteman et al., 2014a). Previous studies in *Xenopus* have demonstrated that Ezrin-depleted MCCs exhibit a very similar phenotype to the one we observed in Crb3.L-depleted MCCs (Epting et al., 2015).

Thus, we hypothesized that Crb3.L might affect the expression and/or the subcellular localization of activated Ezrin. As a first step to evaluate this possibility, we analyzed the localization of phospho-activated ERM during MCC differentiation. pERM expression was detectable in the protruding membrane of MCC starting their insertion into the outer layer (Figure 5 St18, supplementary figure 4). At this stage, pERM staining was also detected in close proximity to the ascending centrioles/BBs, (supplementary figure 4 stage 21). As apical expansion proceeded, pERM formed bright patches on the expanding apical surface (Figure 5 St22, 25), then the patches coalesced in a more structured network superimposed on the mature actin meshwork (Figure 5 St25-30). Accumulation of pERM at cell-cell junctions was observed only in fully mature cells (Figure 5 St 30).

Crb3.L regulates the localization of pERM at the apical membrane

The similar apical distribution of Crb3L and pERM suggests that Crb3.L could control the localization of activated pERM to regulate the nascent actin network during apical expansion. We thus compared the distribution of pERM in control and Crb3.L-depleted immature MCCs undergoing

apical expansion. Crb3.L depletion induced a 33,2% (+/-11 sd) decrease of apical pERM signal intensity (figure 6 A, B, D).

In correlation with this effect, Crb3.L depletion provoked a 30 % (+/- 10 sd) decrease in the average apical medial surface of newly emerged cells. These results are in contrast to the apparently preserved area of stage 28 morphant MCCs (figure 4 N, figure 6 C), and suggest that non-Crb3.L-dependent processes might rescue the initial defect in apical expansion.

These data advocate for Crb3.L being required for regulating pERM on the emerging apical surface of MCCs, so as to bridge newly formed actin filaments to the apical plasma membrane, and promote early apical expansion.

Crb3.L is present on a subset of Rab11a positive endosomes

Besides its function at the apical cytocortex, Crb3.L striking abundance in the vicinity of the BBs as well as the BBs migration defect induced by Crb3.L depletion, suggest that Crb3.L vesicles trafficking might mediate BBs ascension. In several model systems, Crb colocalizes with Rab11 endosomes that are pivotal actor of apical trafficking and required for Crb apical delivery (Aguilar-Aragon et al., 2020; Bo et al., 2023; Buck et al., 2023; Iioka et al., 2019; Schlüter et al., 2009). In addition, Rab11a accumulate in the subapical domain of MCCs at the time of their intercalation (Kim et al., 2012). To ascertain the hypothesis that BBs migration defect could be linked to Crb3.L defective apical vesicular trafficking, we checked if Crb3.L also label Rab11a positive endosomes. During MCCs insertion and early apical surface expansion, detection of endogenous Rab11a via immunofluorescence shows that Rab11a endosomes are closed to ascending centrioles/BBs (figure 7 A-B'). Moreover, Crb3.L labelling, by means of endogenous or HA tagged construct detection, partially colocalizes with Rab11a staining (figure 7 A-B'). These data suggest that some aspects of Crb3.L function in MCC could be mediated by Rab11a positive endosomes at centrioles/BBs.

Rab11 depletion phenocopies Crb3.L loss of function in MCCs.

To test if Rab11a positive endosomes trafficking was required for centrioles/BBs ascension in MCCs we performed Rab11a loss of function experiments using a well characterized morpholino (Kim et al., 2012) and examine MCC phenotype in stage 28 embryos when MCCs are normally fully mature. Rab11a depletion led to a strong centrioles/BBs migration defect: centrioles/BBs aggregated in the cytoplasm or were unevenly distributed at the apical surface (figure 8, C, D, F, G). The apical meshwork formation was affected in Rab11a depleted MCC with a 26% decrease in actin density between Rab11a morpholino injected cell and noninjected cells in mosaic morphants for a morpholino dose of 22 ng. This phenotype was more drastic with 30 ng of Rab11a morpholino leading to a 52% diminution of actin density between Rab11a morpholino injected and noninjected

cells in mosaic morphants. The size of the apical medial domain was also decreased upon Rab11a depletion, with a reduction of about 25% between Rab11a morpholino injected and noninjected cells in mosaic morphants injected with a dose of 22 ng, and 40% between Rab11a morpholino injected and noninjected cells in mosaic morphants injected with a dose of 30 ng. Thus, the phenotypes of Rab11a and Crb3.L depleted MCCs are very similar with respect to BBs migration defect and apical actin meshwork formation. We found that the reduction of the size of the apical medial domain is more pronounced with Rab11a depletion as it persists in mature MCCs. All together, these data support the hypothesis that Crb3.L-Rab11a vesicles mediated apical trafficking is required for BBs ascension, apical expansion and apical actin meshwork formation.

Discussion

In this study, thanks to newly custom-made polyclonal antibodies, we show that the *crb3.L* homeolog is highly expressed in MCCs, with a dynamic pattern of expression at the nexus of BBs and the intensively remodeling cytoskeleton of microtubules and actin. Crb3.L-depleted MCCs displayed a complex phenotype associating BB migration defects, reduction in the apical surface, disorganization of the apical actin meshwork, thus precluding normal ciliogenesis. We further unveil the transient association of endogenous activated ERM with ascending centrioles/BBs and its recruitment to the growing apical surface during the last step of MCCs intercalation. The loss of apical enrichment of pERM paralleled the initial reduction in apical domain expansion in Crb3.L-depleted MCCs. Our data advocate for Crb3.L anchoring Ezrin in an open active conformation at the apical surface of MCCs, thus allowing coordinated growth of the apical membrane with extensive actin cytoskeleton remodeling.

Crb3 homeolog expression in the *Xenopus* mucociliary epidermis

So far, studies addressing the question of Crb3 tissue and subcellular localization in *Xenopus laevis* relied on the expression of a C-terminally GFP-tagged version of *Xenopus tropicalis* Crb3. The amino acid sequence of *Xenopus tropicalis* Crb3 displays 83 and 81% identity with Crb3.L and Crb3.S respectively (Chalmers et al., 2005; Wang et al., 2013, p. 6). This construct allowed the description of the dynamic changes in Crb3 subcellular localization during differentiation and morphogenesis of the non-neural ectoderm, but did not address the function of endogenous Crb3. To determine which homeolog was predominantly expressed in MCCs, and to describe their subcellular localization, antibodies targeting each one of the proteins were generated and we controlled their specificity by immunizing peptide competition assays and loss of function experiment for Crb3.L. These new antibodies allowed us to unveil the distinct but complementary expression of Crb3.L and Crb3.S in

the developing mucociliary epidermis of *Xenopus laevis* embryos, supporting a division of labor scenario following gene duplication.

We confirm that a large pool of Crb3, namely Crb3.S, is indeed located in numerous small intracellular vesicles (Wang et al., 2013). Moreover, the progressive restriction of the endogenous Crb3.S to the outer layer at the time of its mucociliary differentiation is in accordance with the published pattern based on the expression of *tropicalis* Crb3-GFP (Wang et al., 2013). These data advocate that Crb3.S is a marker signing the beginning of the differentiation of the mucociliary epidermis. Later on, the expression of Crb3.S became very variable among the different cell types and surprisingly extremely high in the SSC.

To date, very few SSC markers have been described and they are either transcription factors such as Foxa1, or secreted compounds (Otogelin-like, HNK1, IPTKb, serotonin, Xpod) (Dubaissi et al., 2014; Kurrle et al., 2020; Walentek et al., 2014). Thus Crb3.S is, so far, the sole transmembrane protein described to be highly expressed in SSCs. It extends the short list of bona fide SSC markers, and offers the unique advantage to visualize cell shape via endogenous staining of vesicles and cytoplasmic membranes.

The SSCs are central to the epithelial anti-infective barrier function in *Xenopus laevis* embryos via secretion of anti-microbial substances (Dubaissi et al., 2014; Walentek et al., 2014). Therefore, it would be interesting to study the impact of Crb3.S depletion on the secretory function of the SCC as well as its functional consequences on innate immunity.

Until now, Crb3 localization in ciliated cells focused on its localization in the shaft of primary cilia (Fan et al., 2007, 2004b; Hazime and Malicki, 2017; Sfakianos et al., 2007). Accordingly, functional studies on Crb3 revealed its function in the regulation of intraciliary transport (Fan et al., 2004b; Hazime and Malicki, 2017; Sfakianos et al., 2007) and ciliary membrane composition (Hazime and Malicki, 2017). Here, we do observe a spotty staining of Crb3.L along the axoneme, suggesting that Crb3.L might also regulate ciliary transport/ciliary shaft composition in motile cilia of MCCs.

Before being detected in cilia, Crb3.L accumulates in the sub-apical domain of the intercalating MCCs, in the vicinity of the ascending centrioles/BBs, as well as the newly expanding apical membrane. These subcellular localization data are well in accordance with the compound phenotype we observed: the association of defective centriole/BB ascension, alteration of the apical actin meshwork and apical surface reduction. These data suggest that in MCCs, Crb3 is not exclusively required for ciliary transport, as it has been described for primary cilia (Fan et al., 2004b; Hazime and Malicki, 2017; Sfakianos et al., 2007). Our work points that Crb3.L is likely an iterative player of the stepwise process of multiciliogenesis, being subsequently required for centriole/BB ascension, BB anchoring/fusion to the apical membrane, apical actin meshwork construction, and finally cilia building/maintenance.

Crb3.L- Rab11a doubly labelled vesicles might cooperate for centrioles/BB ascension

We observed a partial co localization of Crb3 and Rab11a labelling in a sub population of vesicles that are very close to BBs in inserting MCCs or MCCs initiating expansion of their apical surface. Moreover, Rab11a depletion alters BBs ascension as in Crb3.L morphant MCCs. Thus Crb3.L might regulate centrioles/BBs ascension through its interaction with the Rab11a apical trafficking endosome. Crb3.L-Rab11a positive endosomes might recruit molecular motors required for the centrioles/BBs ascension process. Crb3.L-Rab11a positive endosomes could also deliver specific regulatory proteins or structural cargos to ascending centrioles/BBs. Accordingly, Bo et al. demonstrated very recently that Crb3.L-Rab11 positive endosomes were carrying components of the γ-Tubulin complex to the basal body of cells bearing primary cilium (Bo et al., 2023).

Crb3.L might coordinate apical membrane expansion with the growth of the apical actin cytocortex

A widely accepted function of Crumbs is to control the size of the apical domain in various model systems *in vivo*. In *Drosophila*, Crb loss-of-function leads to smaller apical surfaces of tracheal and pupal wing cells (Salis et al., 2017a; Skouloudaki et al., 2019). Crb might also selectively participate to the expansion of apical domain subdivision such as the stalk and rhabdomere regions of *Drosophila* photoreceptors, the inner segment of the photoreceptor and the apical microvilli-like protrusions of mechano-sensory neurons in zebrafish, and the microvilli of enterocytes in mice (Charrier et al., 2015a; Desban et al., 2019; Omori and Malicki, 2006; Pellikka et al., 2002; Richard et al., 2009; Whiteman et al., 2014a). In summary, Crb is required for apical growth in tissues undergoing intense morphogenetic events.

In *Xenopus laevis,* overexpression of Crb3 leads to expansion of the apical domain of epithelial cells in the early embryo (Chalmers et al., 2005). However, the question of Crb3 contribution to the very dynamic process of the MCC apical expansion has not been evaluated. Here, we show that prior to apical MCC expansion, Crb3.L labels vesicles accumulating in the subapical domain of inserting cells. Further on, Crb3.L relocates from this vesicular pool to the apical membrane at the time of apical expansion. Thus Crb3.L+ vesicles are ideally positioned for the fast delivery of a ready-made stock of membrane dedicated to apical membrane expansion.

Crb3.L depletion causes an initial reduction of the apical surface in association with decreased levels of F-actin and pERM at the apical cell aspect. MCC apical surface expansion is autonomously driven by 2D pressure powered by the apical medial F-actin pool (Sedzinski et al., 2016). Ezrin depletion in the *Xenopus* multiciliated epithelia leads to profound actin meshwork disorganization (Epting et al., 2015; Yasunaga et al., 2022). The Crb juxta membrane FERM binding domain (FBM domain) binds to the FERM domain of ERM (Médina et al., 2002; Wei et al., 2015; Whiteman et al., 2014a). In the ovarian follicle epithelium of *Drosophila*, Crb with nonfunctional FBM

domain does not stabilize the activated ERM Moesin in the subapical region resulting in the loss of filamentous actin (Sherrard and Fehon, 2015). Thus, in MCCs, Crb3.L might regulate phosphorylated Ezrin in the growing apical domain, allowing progressive growth of the actin meshwork in coordination with apical membrane delivery.

Crb3.L functional complexity in MCCs

We showed that, in immature MCCs, Crb3.L vesicles first accumulate in the vicinity of ascending centrioles/BBs, where they display a partial co-distribution with Rab11a endosomes. Consistently, both Crb3.L and Rab11a loss of function caused defective apical migration of centrioles/BBs. At a later stage, Crb3.L is re-localized from the internal vesicular pool to the apical membrane of the emerging MCC. Consistently, in Crb3.L-depleted cells the apical actin meshwork is defective and pERM staining is decreased. Strikingly, in *Xenopus* MCCs, apical cytoskeleton organization and centriole/BB migration appear tightly coordinated (Ioannou et al., 2013; Nommick et al., 2022). It is therefore difficult to ascertain whether Crb3.L function is restricted to centriole migration, to cytocortex organization or both. Answering this question would require new tools, to discriminate the functions of the distinct Crb3.L pools in live embryos. As an example, light-induced clustering elegantly demonstrated that Rab11 endosomes contribute to left-right organizer lumen formation in zebrafish (Aljiboury et al., 2023; Rathbun et al., 2020). Deeper resolution of the molecular mechanisms at play might also be achieved by proximity labeling strategies. As an illustration, the APEX2 proximity ligation assay allowed the molecular mapping of a Crumbs3 specific subcellular domain in MDCK cells (Tan et al., 2020). Further work based on such new tools may help to elucidate the function of distinct Crb3.L pools in MCCs.

In conclusion, our work unveils a new aspect of Crb3 function in multiciliogenesis in vertebrates. At the tissue level, Crb3 was shown to be required for the differentiation of the proximal airway mucociliary epithelium, including MCC progenitors (Szymaniak et al., 2015). Consequently, MCCs and a fortiori cilia are absent from the proximal airway of lung targeted *crb3* knock-out mice (Szymaniak et al., 2015). This likely explains the respiratory distress syndrome of germline *crb3* knock-out mice (Charrier et al., 2015b; Szymaniak et al., 2015; Whiteman et al., 2014b). In our model, MCCs are present, but display abnormal ciliary tuft, suggesting that Crb3.L is dispensable for MCC specification in the *Xenopus* mucociliary epithelium.

At the cellular level, Crb3 appears to be involved in ciliary trafficking in MCCs as suggested by the cilia phenotype of *crb3* null zebrafish mutants (Hazime and Malicki, 2017). In our model, a ciliary trafficking defect is not excluded, but was not possible to test here as centrioles/BBs were not docked at the apical membrane. Thus Crb3 dependent trafficking seems to be iteratively reemployed

during multiciliogenesis first for centrioles/BB ascension possibly via cooperation with Rab11 apical trafficking endosomes, next in cilia elongation/maintenance via interactions with intraflagellar transport (Hazime and Malicki, 2017; Sfakianos et al., 2007).

Materials and methods

Ethics Statement

All experiments were performed following the Directive 2010/63/EU of the European parliament and of the council of 22 September 2010 on the protection of animals used for scientific purposes and approved by the "Direction départementale de la Protection des Populations, Pôle Alimentation, Santé Animale, Environnement, d'Ille et Vilaine" (agreement number 7257)

Xenopus embryo injections

Wild-type or albino *Xenopus laevis* females were obtained from Biological Resources Center (CRB France or NASCO, USA). Eggs were fertilized *in vitro,* and embryos were de-jellied and reared as previously described (Nommick et al., 2022). For microinjections, embryos were placed in a 5% Ficoll buffered solution (Hatte et al., 2018; Nommick et al., 2022). To specifically target the epidermis, 8-cells embryos were injected in a ventral blastomere of the animal pole. For depletion experiments, embryos were injected with 15 or 30 ng of *5'UTR-crb3.L-mo* or *ATG-crb3.L-mo* respectively, together with 200 pg of *gfp-gpi* mRNA. For rescue experiments, *5'UTR-crb3.L-mo* was co-injected with 200 pg of *mrfp-caax* mRNA and the HA tagged resistant *crb3.L* mRNA.

Cloning of crb3.L and crb3.S, constructs, mRNA, morpholinos®

Predictive ORFs of *crb3.L* and *crb3.S* of *Xenopus laevis* were identified by comparing genomic, RNA and protein sequences of *Xenopus tropicalis* and *Xenopus laevis,* as well as using the annotated versions of the genomes (Xenbase). cDNAs were prepared via reverse transcription (SuperSriptIII first strand synthesis, Invitrogen) from RNA extracted with silica membrane column purification (PureLink RNA mini kit Thermofisher). The following primer were used to amplify the coding sequences of each gene.

forward primer *crb3.L:5'*- CTCTGCGTCCCTACCCTG-3'

reverse primer *crb3.L*: 5'TGTAAGGCGCAGTTTTGACC-3'

forward primer *crb3.S:* 5'-CAGGCTGATCTCTGCATCAC-3'

reverse primer *crb3.S:* 5'-AGGAATCTCTCCTGGAGTTCA-3'

PCR fragments were purified and cloned into pGEM-T Easy+, and subcloned in pCS2+ using the EcoR I cloning site to obtain the 29bp-*crb3.L*-pCS2+ vector, 29 bp of the 5'UTR were present in this first

construct. The HA tagged *crb3.L* rescue construct resistant to 5'UTR morpholino, (HA-*crb3.L*-pCS2+), was constructed as follows. First, the HA epitope sequence was inserted immediately 3' to the signal peptide sequence by site directed mutagenesis using the QuickchangeXL site directed Mutagenesis kit (Agilent) to obtain the following intermediate vector: 29bp-HA-*crb3.L*-pCS2+. To this end the following primers were used:

forward primer HAmut*crb3.L*:

5'-CCTGTCATTAGTGAAAGCTTACCCATACGATGTTCCAGATTACGCTCAGAATGTCACCACTTCAG-3'

reverse primer HAmut*crb3.L*:

5'-CTGAAGTGGTGACATTCTGAGCGTAATCTGGAACATCGTATGGGTAAGCTTTCACTAATGACAGG-3'

The insertion of an optimal Kozak sequence with simultaneous deletion of the 5'UTR remnant were performed by PCR using as a template the restriction fragment obtained by the digestion of 29bp-HA-*crb3.L*-pCS2+ by EcoRI.

The following primers were used.

forward 5' GAGAGAATTCCGCCACCATGCTCGATTATCTA

reverse primer 5'GAGACTCGAGACTAGTGATTTGTAAGGCGC.

PCR fragments were digested, purified and cloned into PCS2+ using the EcorI-XhoI cloning sites. Accuracy of the sequences were verified by sequencing.

The plasmids encoding tracers: PCS2+-RFP-caax, PCS2+-GFP-GPI were from lab stocks. PCS107-GFP-CP110 was a kind gift of Peter Walentek (Center for biological system analysis Universitätsklinikum Freiburg, Freiburg, Germany).

Linearized plasmids were used as template for *in vitro* synthesis of mRNA using the SP6 m message machine kit (Ambion) and purified using the Megaclear Kit (Life technology Ambion).

Two independent morpholinos® were designed targeting either the 5'UTR of *crb3.L*, named *5'UTR-crb3.L-mo*, encoded by 5'-ACAGTAACAGGGTAGGGACGCA-3' or the translational initiation codon named *ATG-crb3.L-mo* encoded by 5'-TTAGTAGATAATCGAGCATGTGGAC-3'. The sequence of morpholino targeting the translation initiation codon of the two *Rab11a* homeologs was 5'-TAC CCA TCG TCG CGG CAC TTC TGAC-3' as in (Kim et al., 2012).

Immunohistochemistry

Embryos were staged and arrested at appropriated stages according to Faber and Nieuwkoop (Faber and Nieuwkoop, 2020). For stage 21-22 embryos were incubated at 13°c until late afternoon the day of injection and then placed at 16°c for 2 days. For stage 28, embryos were incubated at 13°c for 4 days. For embryos that did not hatch, the vitelline membrane was manually removed with tweezers before proceeding to fixation. Fixation conditions varied according to the antibodies and/or the probes (see tables S1-3). After fixation, embryos were immunostained *in toto*, or further processed

for cryosections. Cryopreservation was achieved by incubation in serial graded sucrose solutions (5 to 30%). Embryos were then embedded in Optimal Cut Temperature medium (OCT VWR chemicals), snap frozen in a dry ice ethanol bath, and stored at-80°C, 5 to 10 µm thick cryosections were obtained with cryostat.

For whole mount immunostaining, buffers and detergents varied with the antibodies or probes. For staining including p-ERM and SiR actin, embryos were washed in a tris buffer saline (TBS) NP-40 0,05% solution, and blocked in TBS-NP40 0,05% with 15% fetal calf serum (FCS). For the other staining, embryos were washed in maleic acid and triton 0,1% (MABX), and blocked in MABX with 15% FCS.

Information's about the antibodies, fixation conditions, specific changes regarding the following general immunofluorescence protocol are provided in the supplementary section (tables S1-3).

Next, embryos were usually incubated overnight at 4°C with the first antibodies (see table S1). Embryos were then extensively washed for 4 to 6 hours, incubated 30 minutes to 1 hour in blocking buffer, then transferred in the solution containing the appropriate combination of goat secondary alexa-fluor coupled antibodies at 1/500 for 1h30-2 hours (see table S2). After incubation, embryos were shortly washed and mounted in antifading medium (mowiol-DABCO) between slide and coverslip. Exceptions to this protocol were the increased incubation time for anti-Crb3 antibodies (3-4 days, 4°C), addition of SiR-actin 1/1000 to the fixative solution (1 hours) and with the secondary antibodies (1h30 hours) (see table S3).

For Crb3.L immunostaining on cryosections, reagents and conditions were the same as described above. Peanut agglutinin (PNA) was incubated on the slide for 15 minutes after the secondary antibody incubation and wash (see table S3).

Generation of Crb3 homeolog L and S specific antibodies.

Crb3 homeolog L and S specific antibodies were obtained by immunizing rabbits using the speedy protocol from Eurogentec (Seraing, Belgium). The synthetic peptides identical to the ectodomain of Crb3.L (H-QNVTTSAPDRLSESAR-C) or Crb3.S (H-QNVTTPAPGKLSESA-C) were coupled with the KLH (keyhole limpet hemocyanin) carrier protein on their C-terminal part. These peptides were used for affinity purification of the immunized rabbits. Validation of the antibodies was demonstrated via immunizing peptide competition assays for Crb3.L and Crb3.S and depletion through morpholino knockdown for Crb3.L (see supplementary data).

Competition assays were performed using the three following conditions. The antibodies against Crb.3 were incubated overnight at 4 °C with either the immunizing peptide, or an unrelated peptide (QTISDPGEEDPPVSKC present in *Oopsacas minuta* type IV collagen, negative control) or only MABX buffer (positive control). The molar ratio between antibodies and peptides was 1 mol for 25 mol,

respectively, and antibodies were used at 1:200 (2.6 µg/mL). After centrifugation (21,000 g, 4 h, 4 °C) to get rid of potential antibody-peptide complexes, supernatants were used to perform the immunostaining protocol. Incubation of antibodies with the immunizing peptide caused the loss of immunostaining unlike incubation with *Oopsacas minuta* type IV collagen.

Imaging and quantification

Confocal images were acquired using ZEISS LSM 510 and 780, Leica SP5 and SP8 confocal microscopes with 63 x oil objectives. Sequential or simultaneous laser excitations were applied depending on fluorophores, combinations, spectra, staining brightness and persistence.

Basal Bodies

Apically anchored BBs

Centrin staining was used for BBs detection. Apical surfaces of individual MCCs marked by the tracer corresponding to regions of interest (ROI) were segmented manually. Maximum intensity projection of the 3 planes framing the MCCs apical surface was applied to Centrin pictures and converted to 8-bits format. Automated detection of Centrin dots was performed in the ROI using the function find maxima>point selection of Fiji. For this purpose, images were acquired with 63 x oil objective applying a 2,5 zoom and z slice interval of 0,4 µm.

Non apically anchored BBs

Z series were set to frame the totality of the Centrin staining in MCCs. The number of Z-slices containing Centrin dots was used as a proxy for the apico-basal dispersion of BBs in the cytoplasm. These values were converted in distances from the cell apex. For this purpose, images were acquired with 63 x oil objective applying a 2,5 zoom and z slice interval of 0,4 µm.

p-ERM and F-actin signals:

Fluorescence of either signals was measured on 8-bit pictures using the mean gray value function of Fiji on maximal intensity projection of the three most apical cell planes.

The apical medial area delimited by the apical cell-cell junctions but excluding them was used as a proxi for apical surface measures (intensity, size) for either stainings.

p-ERM signal quantification was performed in mosaic tracer-injected control and crb3.L-depleted embryos to circumvent non-biological interindividual variations of the staining intensity. Measures of mean pixel intensity of pERM staining per cell were performed on confocal plane including at least two tracer positive (cti) and negative MCCs (ctni) in control embryos, as well as two 5'UTR-crb3L-mo

+ tracer positive (moi) and negative (moni) MCCs in morphant embryos. Then, the average intensity (mean pixel intensity) of each cell population was calculated for each plane. The absence of variation of the average intensity between cti and ctni was a prerequisite for interpreting a variation between moi and moni.

F-actin staining was quantified in two ways according to the associated stainings. When F-actin staining was coupled with pERM staining, F actin staining was quantified the same way as pERM (see above). When F actin staining was not associated with pERM, medial and junctional actin intensity were measured. The line delimitating the medial domain was the internal limit of the junctional region, the outer limit was automatically drawn by the make band tool of Fiji, fixing thickness of the band at 2µm. As junctional actin does not vary between *5'UTR-Crb3.L* morpholino injected and control cells in mosaic morphants it can be used as reference point for medial actin intensity.

For p-ERM and F-actin stainings, images were acquired with 63 x oil objective and z slice interval of 0,5 µm.

Transmission electron microscopy

Stage 28 Embryos were processed for electron microscopy as previously described (Revinski et al., 2018). 80 nm sections were made with a Leica Ultracut UC7 (Leica, Germany). Images were acquired using a Tecnai G2 (Thermofisher, USA) microscope and a Veleta camera (Olympus Japan).

Statistical analysis

Statistical analyses were performed with RStudio (version 1.4.1717). Before comparing the mean of variables, normality and homoscedasticity were evaluated with Shapiro and Barlett tests, respectively. When data followed normal and homoscedastic distribution, Student's t-test was applied for comparing two groups. When data did not complete these two conditions, non-parametric tests were used. For two-groups comparison, Wilcoxon test was used. For comparison including more than two groups, Kruskal-Wallis tests were used, followed by post hoc Wilcoxon-test with Bonferroni correction to examine differences between two means. Distribution are depicted as Box-plot, box represent the interquartile range (50% of the distribution) and whiskers highlight 1,5 interquartile range, median is shown. Chi-squared test was applied for percentage comparison. For all tests, significance threshold was set at $p<0,05$. * for $p<0,05$, ** for $p<0,01$, *** for $p< 0,005$, **** for $p<0,001$

Funding

This work was supported by the Centre National de la Recherche Scientifique (CNRS)(LK and LBA salaries), the Aix Marseille University (CB salary), the Rennes University (CB salary) and Inserm for GM salary, the ANR grant awarded to LK (ANR-15-CE13-003), to ALB and LK (ANR-14-CE13-0013), and the LabEx INFORM (ANR-11-LABX-0054) to ALB. JR salary was supported by the ANR grant (ANR-11-LABX-0054). Light imaging was performed at the optical imaging and electron microscopy (PiCSL-FBI core facility) platforms of the Institute for Developmental Biology of Marseille (IBDM, France) and at the Microscopy Rennes imaging Center (MRiC, Biosit, Rennes). Electron microscopy experiments were performed at PiCSL-FBI facility. The PiCSL-FBI and MRiC, Biosit facilities are France Bio-Imaging infrastructures, supported by the French National Research Agency (ANR-10-INBS-04).

Acknowledgements

We are grateful to E Bazellières and A Pasini for critical reading of the manuscript. We wish to thank PA Bidaud-Meynard, A Pacquelet, J Pécréaux and JP Tassan for stimulating discussion. We thank P. Walentek for providing the CP110-GFP plasmid. We thank X. Pinson, S. Dutertre, R. Flores-Flores, E. Castellani for their technical assistance with confocal microscopy. We thank F. Roguet and J. Maurais for *Xenopus* care. We thank all members of the Gene Expression and Development team (GED) in particular A. Mereau for her help on Western Blot. We thank J.P. Tassan and V. Thomé for sharing *Xenopus* expertise and/or reagents. We are grateful to R. Gibeaux and C. Callens for offering a safe harbor for *Xenopus* injections during IGDR building renovation.

Conflict of Interest statement: None declared.

Authors contributions: Conceptualization: C.B, L.K, A.LB.; Methodology: C.B., L.K.; Validation: C.B, L.K A.LB; Investigation: C.B, J.R.; Writing - original draft: C.B, A.LB, L.K; Writing-review and editing: C.B, A.LB, L.K, G.M. Supervision: L.K.; A.LB; Project administration: A.LB; Funding acquisition: A.LB, L.K.

References

Adler, P.N., Wallingford, J.B., 2017. From Planar Cell Polarity to Ciliogenesis and Back: The Curious Tale of the PPE and CPLANE proteins. Trends Cell Biol. 27, 379–390. https://doi.org/10.1016/j.tcb.2016.12.001

Aguilar-Aragon, M., Fletcher, G., Thompson, B.J., 2020. The cytoskeletal motor proteins Dynein and MyoV direct apical transport of Crumbs. Dev. Biol. 459, 126–137. https://doi.org/10.1016/j.ydbio.2019.12.009

Aljiboury, A.A., Ingram, E., Krishnan, N., Ononiwu, F., Pal, D., Manikas, J., Taveras, C., Hall, N.A., Da Silva, J., Freshour, J., Hehnly, H., 2023. Rab8, Rab11, and Rab35 coordinate lumen and cilia formation during zebrafish left-right organizer development. PLOS Genet. 19, e1010765. https://doi.org/10.1371/journal.pgen.1010765

Antoniades, I., Stylianou, P., Skourides, P.A., 2014. Making the connection: ciliary adhesion complexes anchor basal bodies to the actin cytoskeleton. Dev. Cell 28, 70–80. https://doi.org/10.1016/j.devcel.2013.12.003

Anvarian, Z., Mykytyn, K., Mukhopadhyay, S., Pedersen, L.B., Christensen, S.T., 2019. Cellular signalling by primary cilia in development, organ function and disease. Nat. Rev. Nephrol. 15, 199–219. https://doi.org/10.1038/s41581-019-0116-9

Apodaca, G., 2018. Role of Polarity Proteins in the Generation and Organization of Apical Surface Protrusions. Cold Spring Harb. Perspect. Biol. 10, a027813. https://doi.org/10.1101/cshperspect.a027813

Bajur, A.T., Iyer, K.V., Knust, E., 2019. Cytocortex-dependent dynamics of Drosophila Crumbs controls junctional stability and tension during germ band retraction. J. Cell Sci. 132, jcs228338. https://doi.org/10.1242/jcs.228338

Bangs, F., Anderson, K.V., 2017. Primary Cilia and Mammalian Hedgehog Signaling. Cold Spring Harb. Perspect. Biol. 9, a028175. https://doi.org/10.1101/cshperspect.a028175

Bazellières, E., Aksenova, V., Barthélémy-Requin, M., Massey-Harroche, D., Le Bivic, A., 2018. Role of the Crumbs proteins in ciliogenesis, cell migration and actin organization. Semin. Cell Dev. Biol. 81, 13–20. https://doi.org/10.1016/j.semcdb.2017.10.018

Bazellieres, E., Assemat, E., Arsanto, J.-P., Bivic, A.L., Massey-Harroche, D., 2009. Crumbs proteins in epithelial morphogenesis. Front. Biosci.-Landmark 14, 2149–2169. https://doi.org/10.2741/3368

Bo, W., Zheyong, L., Tan, T., Miao, Z., Yina, J., Yangyang, S., Xiaoqian, G., Shaoran, S., Ruiqi, W., He, C., Jie, L., Juan, L., Yu, R., Peijun, L., 2023. CRB3 navigates Rab11 trafficking vesicles to promote γTuRC assembly during ciliogenesis. eLife 12. https://doi.org/10.7554/eLife.86689

Boisvieux-Ulrich, E., Lainé, M.-C., Sandoz, D., 1990. Cytochalasin D inhibits basal body migration and ciliary elongation in quail oviduct epithelium. Cell Tissue Res. 259, 443–454. https://doi.org/10.1007/BF01740770

Boisvieux-Ulrich, E., Laine, M.C., Sandoz, D., 1987. In vitro effects of benzodiazepines on ciliogenesis in the quail oviduct. Cell Motil. Cytoskeleton 8, 333–344. https://doi.org/10.1002/cm.970080406

Boutin, C., Kodjabachian, L., 2019. Biology of multiciliated cells. Curr. Opin. Genet. Dev. 56, 1–7. https://doi.org/10.1016/j.gde.2019.04.006

Buck, T.M., Quinn, P.M.J., Pellissier, L.P., Mulder, A.A., Jongejan, A., Lu, X., Boon, N., Koot, D., Almushattat, H., Arendzen, C.H., Vos, R.M., Bradley, E.J., Freund, C., Mikkers, H.M.M., Boon, C.J.F., Moerland, P.D., Baas, F., Koster, A.J., Neefjes, J., Berlin, I., Jost, C.R., Wijnholds, J., 2023. CRB1 is required for recycling by RAB11A+ vesicles in human retinal organoids. Stem Cell Rep. S2213-6711(23)00263–1. https://doi.org/10.1016/j.stemcr.2023.07.001

Buckley, C.E., St Johnston, D., 2022. Apical–basal polarity and the control of epithelial form and function. Nat. Rev. Mol. Cell Biol. 1–19. https://doi.org/10.1038/s41580-022-00465-y

Chalmers, A.D., Pambos, M., Mason, J., Lang, S., Wylie, C., Papalopulu, N., 2005. aPKC, Crumbs3 and Lgl2 control apicobasal polarity in early vertebrate development. Dev. Camb. Engl. 132, 977–986. https://doi.org/10.1242/dev.01645

Charrier, L.E., Loie, E., Laprise, P., 2015a. Mouse Crumbs3 sustains epithelial tissue morphogenesis in vivo. Sci. Rep. 5, 17699. https://doi.org/10.1038/srep17699

Charrier, L.E., Loie, E., Laprise, P., 2015b. Mouse Crumbs3 sustains epithelial tissue morphogenesis in vivo. Sci. Rep. 5, 17699. https://doi.org/10.1038/srep17699

Chuyen, A., Rulquin, C., Daian, F., Thomé, V., Clément, R., Kodjabachian, L., Pasini, A., 2021. The Scf/Kit pathway implements self-organized epithelial patterning. Dev. Cell 56, 795-810.e7. https://doi.org/10.1016/j.devcel.2021.02.026

Clark, A.G., Wartlick, O., Salbreux, G., Paluch, E.K., 2014. Stresses at the Cell Surface during Animal Cell Morphogenesis. Curr. Biol. 24, R484–R494. https://doi.org/10.1016/j.cub.2014.03.059

Collins, C., Kim, S.K., Ventrella, R., Carruzzo, H.M., Wortman, J.C., Han, H., Suva, E.E., Mitchell, J.W., Yu, C.C., Mitchell, B.J., 2021. Tubulin acetylation promotes penetrative capacity of cells undergoing radial intercalation. Cell Rep. 36, 109556. https://doi.org/10.1016/j.celrep.2021.109556

Collins, C., Majekodunmi, A., Mitchell, B., 2020. Centriole Number and the Accumulation of Microtubules Modulate the Timing of Apical Insertion during Radial Intercalation. Curr. Biol. 30, 1958-1964.e3. https://doi.org/10.1016/j.cub.2020.03.013

Deblandre, G.A., Wettstein, D.A., Koyano-Nakagawa, N., Kintner, C., 1999. A two-step mechanism generates the spacing pattern of the ciliated cells in the skin of Xenopus embryos. Development 126, 4715–4728. https://doi.org/10.1242/dev.126.21.4715

Desban, L., Prendergast, A., Roussel, J., Rosello, M., Geny, D., Wyart, C., Bardet, P.-L., 2019. Regulation of the apical extension morphogenesis tunes the mechanosensory response of microvilliated neurons. PLoS Biol. 17, e3000235. https://doi.org/10.1371/journal.pbio.3000235

Dubaissi, E., Papalopulu, N., 2011. Embryonic frog epidermis: a model for the study of cell-cell interactions in the development of mucociliary disease. Dis. Model. Mech. 4, 179–192. https://doi.org/10.1242/dmm.006494

Dubaissi, E., Rousseau, K., Hughes, G.W., Ridley, C., Grencis, R.K., Roberts, I.S., Thornton, D.J., 2018. Functional characterization of the mucus barrier on the Xenopus tropicalis skin surface. Proc. Natl. Acad. Sci. 115, 726–731. https://doi.org/10.1073/pnas.1713539115

Dubaissi, E., Rousseau, K., Lea, R., Soto, X., Nardeosingh, S., Schweickert, A., Amaya, E., Thornton, D.J., Papalopulu, N., 2014. A secretory cell type develops alongside multiciliated cells, ionocytes and goblet cells, and provides a protective, anti-infective function in the frog embryonic mucociliary epidermis. Dev. Camb. Engl. 141, 1514–1525. https://doi.org/10.1242/dev.102426

Epting, D., Slanchev, K., Boehlke, C., Hoff, S., Loges, N.T., Yasunaga, T., Indorf, L., Nestel, S., Lienkamp, S.S., Omran, H., Kuehn, E.W., Ronneberger, O., Walz, G., Kramer-Zucker, A., 2015. The Rac1 regulator ELMO controls basal body migration and docking in multiciliated cells through interaction with Ezrin. Dev. Camb. Engl. 142, 174–184. https://doi.org/10.1242/dev.112250

Faber, J., Nieuwkoop, P.D. (Eds.), 2020. Normal Table of Xenopus Laevis (Daudin): A Systematical and Chronological Survey of the Development from the Fertilized Egg Till the End of Metamorphosis. Garland Science, New York. https://doi.org/10.1201/9781003064565

Fan, S., Fogg, V., Wang, Q., Chen, X.-W., Liu, C.-J., Margolis, B., 2007. A novel Crumbs3 isoform regulates cell division and ciliogenesis via importin beta interactions. J. Cell Biol. 178, 387–398. https://doi.org/10.1083/jcb.200609096

Fan, S., Hurd, T.W., Liu, C.-J., Straight, S.W., Weimbs, T., Hurd, E.A., Domino, S.E., Margolis, B., 2004a. Polarity proteins control ciliogenesis via kinesin motor interactions. Curr. Biol. CB 14, 1451–1461. https://doi.org/10.1016/j.cub.2004.08.025

Fan, S., Hurd, T.W., Liu, C.-J., Straight, S.W., Weimbs, T., Hurd, E.A., Domino, S.E., Margolis, B., 2004b. Polarity proteins control ciliogenesis via kinesin motor interactions. Curr. Biol. CB 14, 1451–1461. https://doi.org/10.1016/j.cub.2004.08.025

Fehon, R.G., McClatchey, A.I., Bretscher, A., 2010. Organizing the cell cortex: the role of ERM proteins. Nat. Rev. Mol. Cell Biol. 11, 276–287. https://doi.org/10.1038/nrm2866

Flores-Benitez, D., Knust, E., 2015. Crumbs is an essential regulator of cytoskeletal dynamics and cell-cell adhesion during dorsal closure in Drosophila. eLife 4, e07398. https://doi.org/10.7554/eLife.07398

Gao, Y., Lui, W., Lee, W.M., Cheng, C.Y., 2016. Polarity protein Crumbs homolog-3 (CRB3) regulates ectoplasmic specialization dynamics through its action on F-actin organization in Sertoli cells. Sci. Rep. 6, 28589. https://doi.org/10.1038/srep28589

Haas, M., Vázquez, J.L.G., Sun, D.I., Tran, H.T., Brislinger, M., Tasca, A., Shomroni, O., Vleminckx, K., Walentek, P., 2019. ΔN-Tp63 Mediates Wnt/β-Catenin-Induced Inhibition of Differentiation in Basal Stem Cells of Mucociliary Epithelia. Cell Rep. 28, 3338-3352.e6. https://doi.org/10.1016/j.celrep.2019.08.063

Hatte, G., Prigent, C., Tassan, J.-P., 2018. Tight junctions negatively regulate mechanical forces applied to adherens junctions in vertebrate epithelial tissue. J. Cell Sci. 131, jcs208736. https://doi.org/10.1242/jcs.208736

Hazime, K., Malicki, J.J., 2017. Apico-basal Polarity Determinants Encoded by crumbs Genes Affect Ciliary Shaft Protein Composition, IFT Movement Dynamics, and Cilia Length. Genetics 207, 1041–1051. https://doi.org/10.1534/genetics.117.300260

Herawati, E., Taniguchi, D., Kanoh, H., Tateishi, K., Ishihara, S., Tsukita, S., 2016. Multiciliated cell basal bodies align in stereotypical patterns coordinated by the apical cytoskeleton. J. Cell Biol. 214, 571–586. https://doi.org/10.1083/jcb.201601023

Iioka, H., Saito, K., Kondo, E., 2019. Crumbs3 regulates the expression of glycosphingolipids on the plasma membrane to promote colon cancer cell migration. Biochem. Biophys. Res. Commun. 519, 287–293. https://doi.org/10.1016/j.bbrc.2019.08.161

Ioannou, A., Santama, N., Skourides, P.A., 2013. Xenopus laevis nucleotide binding protein 1 (xNubp1) is important for convergent extension movements and controls ciliogenesis via regulation of the actin cytoskeleton. Dev. Biol. 380, 243–258. https://doi.org/10.1016/j.ydbio.2013.05.004

Kerman, B.E., Cheshire, A.M., Myat, M.M., Andrew, D.J., 2008. Ribbon Modulates Apical Membrane during Tube Elongation through Crumbs and Moesin. Dev. Biol. 320, 278–288. https://doi.org/10.1016/j.ydbio.2008.05.541

Kim, K., Lake, B.B., Haremaki, T., Weinstein, D.C., Sokol, S.Y., 2012. Rab11 regulates planar polarity and migratory behavior of multiciliated cells in Xenopus embryonic epidermis. Dev. Dyn. 241, 1385–1395. https://doi.org/10.1002/dvdy.23826

Knödler, A., Feng, S., Zhang, J., Zhang, X., Das, A., Peränen, J., Guo, W., 2010. Coordination of Rab8 and Rab11 in primary ciliogenesis. Proc. Natl. Acad. Sci. U. S. A. 107, 6346–6351. https://doi.org/10.1073/pnas.1002401107

Kurrle, Y., Kunesch, K., Bogusch, S., Schweickert, A., 2020. Serotonin and MucXS release by small secretory cells depend on Xpod, a SSC specific marker gene. genesis 58, e23344. https://doi.org/10.1002/dvg.23344

Lemullois, M., Boisvieux-Ulrich, E., Laine, M.C., Chailley, B., Sandoz, D., 1988. Development and functions of the cytoskeleton during ciliogenesis in metazoa. Biol. Cell 63, 195–208. https://doi.org/10.1016/0248-4900(88)90058-5

Letizia, A., Sotillos, S., Campuzano, S., Llimargas, M., 2011. Regulated Crb accumulation controls apical constriction and invagination in Drosophila tracheal cells. J. Cell Sci. 124, 240–251. https://doi.org/10.1242/jcs.073601

Mahuzier, A., Shihavuddin, A., Fournier, C., Lansade, P., Faucourt, M., Menezes, N., Meunier, A., Garfa-Traoré, M., Carlier, M.-F., Voituriez, R., Genovesio, A., Spassky, N., Delgehyr, N., 2018. Ependymal cilia beating induces an actin network to protect centrioles against shear stress. Nat. Commun. 9, 2279. https://doi.org/10.1038/s41467-018-04676-w

Médina, E., Williams, J., Klipfell, E., Zarnescu, D., Thomas, G., Le Bivic, A., 2002. Crumbs interacts with moesin and beta(Heavy)-spectrin in the apical membrane skeleton of Drosophila. J. Cell Biol. 158, 941–951. https://doi.org/10.1083/jcb.200203080

Mitchell, B., Jacobs, R., Li, J., Chien, S., Kintner, C., 2007. A positive feedback mechanism governs the polarity and motion of motile cilia. Nature 447, 97–101. https://doi.org/10.1038/nature05771

Nommick, A., Boutin, C., Rosnet, O., Schirmer, C., Bazellières, E., Thomé, V., Loiseau, E., Viallat, A., Kodjabachian, L., 2022. Lrrcc1 and Ccdc61 are conserved effectors of multiciliated cell function. J. Cell Sci. 135, jcs258960. https://doi.org/10.1242/jcs.258960

Omori, Y., Malicki, J., 2006. oko meduzy and Related crumbs Genes Are Determinants of Apical Cell Features in the Vertebrate Embryo. Curr. Biol. 16, 945–957. https://doi.org/10.1016/j.cub.2006.03.058

Park, T.J., Haigo, S.L., Wallingford, J.B., 2006. Ciliogenesis defects in embryos lacking inturned or fuzzy function are associated with failure of planar cell polarity and Hedgehog signaling. Nat. Genet. 38, 303–311. https://doi.org/10.1038/ng1753

Park, T.J., Mitchell, B.J., Abitua, P.B., Kintner, C., Wallingford, J.B., 2008. Dishevelled controls apical docking and planar polarization of basal bodies in ciliated epithelial cells. Nat. Genet. 40, 871–879. https://doi.org/10.1038/ng.104

Pelaseyed, T., Bretscher, A., 2018. Regulation of actin-based apical structures on epithelial cells. J. Cell Sci. 131, jcs221853. https://doi.org/10.1242/jcs.221853

Pellikka, M., Tanentzapf, G., Pinto, M., Smith, C., McGlade, C.J., Ready, D.F., Tepass, U., 2002. Crumbs, the Drosophila homologue of human CRB1/RP12, is essential for photoreceptor morphogenesis. Nature 416, 143–149. https://doi.org/10.1038/nature721

Quigley, I.K., Stubbs, J.L., Kintner, C., 2011. Specification of ion transport cells in the Xenopus larval skin. Dev. Camb. Engl. 138, 705–714. https://doi.org/10.1242/dev.055699

Rathbun, L.I., Colicino, E.G., Manikas, J., O'Connell, J., Krishnan, N., Reilly, N.S., Coyne, S., Erdemci-Tandogan, G., Garrastegui, A., Freshour, J., Santra, P., Manning, M.L., Amack, J.D., Hehnly, H., 2020. Cytokinetic bridge triggers de novo lumen formation in vivo. Nat. Commun. 11, 1269. https://doi.org/10.1038/s41467-020-15002-8

Reiter, J.F., Leroux, M.R., 2017. Genes and molecular pathways underpinning ciliopathies. Nat. Rev. Mol. Cell Biol. 18, 533–547. https://doi.org/10.1038/nrm.2017.60

Revinski, D.R., Zaragosi, L.-E., Boutin, C., Ruiz-Garcia, S., Deprez, M., Thomé, V., Rosnet, O., Gay, A.-S., Mercey, O., Paquet, A., Pons, N., Ponzio, G., Marcet, B., Kodjabachian, L., Barbry, P., 2018. CDC20B is required for deuterosome-mediated centriole production in multiciliated cells. Nat. Commun. 9, 4668. https://doi.org/10.1038/s41467-018-06768-z

Richard, M., Muschalik, N., Grawe, F., Özüyaman, S., Knust, E., 2009. A role for the extracellular domain of Crumbs in morphogenesis of Drosophila photoreceptor cells. Eur. J. Cell Biol. 88, 765–777. https://doi.org/10.1016/j.ejcb.2009.07.006

Rodriguez-Boulan, E., Macara, I.G., 2014. Organization and execution of the epithelial polarity programme. Nat. Rev. Mol. Cell Biol. 15, 225–242. https://doi.org/10.1038/nrm3775

Román-Fernández, A., Bryant, D.M., 2016. Complex Polarity: Building Multicellular Tissues Through Apical Membrane Traffic. Traffic 17, 1244–1261. https://doi.org/10.1111/tra.12417

Röper, K., 2012. Anisotropy of Crumbs and aPKC Drives Myosin Cable Assembly during Tube Formation. Dev. Cell 23, 939–953. https://doi.org/10.1016/j.devcel.2012.09.013

Salis, P., Payre, F., Valenti, P., Bazellieres, E., Le Bivic, A., Mottola, G., 2017a. Crumbs, Moesin and Yurt regulate junctional stability and dynamics for a proper morphogenesis of the Drosophila pupal wing epithelium. Sci. Rep. 7, 16778. https://doi.org/10.1038/s41598-017-15272-1

Salis, P., Payre, F., Valenti, P., Bazellieres, E., Le Bivic, A., Mottola, G., 2017b. Crumbs, Moesin and Yurt regulate junctional stability and dynamics for a proper morphogenesis of the Drosophila pupal wing epithelium. Sci. Rep. 7, 16778. https://doi.org/10.1038/s41598-017-15272-1

Saotome, I., Curto, M., McClatchey, A.I., 2004. Ezrin is essential for epithelial organization and villus morphogenesis in the developing intestine. Dev. Cell 6, 855–864. https://doi.org/10.1016/j.devcel.2004.05.007

Schlüter, M.A., Pfarr, C.S., Pieczynski, J., Whiteman, E.L., Hurd, T.W., Fan, S., Liu, C.-J., Margolis, B., 2009. Trafficking of Crumbs3 during cytokinesis is crucial for lumen formation. Mol. Biol. Cell 20, 4652–4663. https://doi.org/10.1091/mbc.e09-02-0137

Schottenfeld-Roames, J., Rosa, J.B., Ghabrial, A.S., 2014. Seamless tube shape is constrained by endocytosis-dependent regulation of active Moesin. Curr. Biol. CB 24, 1756–1764. https://doi.org/10.1016/j.cub.2014.06.029

Sedzinski, J., Hannezo, E., Tu, F., Biro, M., Wallingford, J.B., 2017. RhoA regulates actin network dynamics during apical surface emergence in multiciliated epithelial cells. J. Cell Sci. 130, 420–428. https://doi.org/10.1242/jcs.194704

Sedzinski, J., Hannezo, E., Tu, F., Biro, M., Wallingford, J.B., 2016. Emergence of an Apical Epithelial Cell Surface In Vivo. Dev. Cell 36, 24–35. https://doi.org/10.1016/j.devcel.2015.12.013

Sfakianos, J., Togawa, A., Maday, S., Hull, M., Pypaert, M., Cantley, L., Toomre, D., Mellman, I., 2007. Par3 functions in the biogenesis of the primary cilium in polarized epithelial cells. J. Cell Biol. 179, 1133–1140. https://doi.org/10.1083/jcb.200709111

Sherrard, K.M., Fehon, R.G., 2015. The transmembrane protein Crumbs displays complex dynamics during follicular morphogenesis and is regulated competitively by Moesin and aPKC. Dev. Camb. Engl. 142, 1869–1878. https://doi.org/10.1242/dev.115329

Simões, S., Lerchbaumer, G., Pellikka, M., Giannatou, P., Lam, T., Kim, D., Yu, J., Ter Stal, D., Al Kakouni, K., Fernandez-Gonzalez, R., Tepass, U., 2022. Crumbs complex-directed apical membrane dynamics in epithelial cell ingression. J. Cell Biol. 221, e202108076. https://doi.org/10.1083/jcb.202108076

Skouloudaki, K., Papadopoulos, D.K., Tomancak, P., Knust, E., 2019. The apical protein Apnoia interacts with Crumbs to regulate tracheal growth and inflation. PLOS Genet. 15, e1007852. https://doi.org/10.1371/journal.pgen.1007852

Spassky, N., Meunier, A., 2017. The development and functions of multiciliated epithelia. Nat. Rev. Mol. Cell Biol. 18, 423–436. https://doi.org/10.1038/nrm.2017.21

Stubbs, J.L., Davidson, L., Keller, R., Kintner, C., 2006. Radial intercalation of ciliated cells during Xenopus skin development. Development 133, 2507–2515. https://doi.org/10.1242/dev.02417

Szymaniak, A.D., Mahoney, J.E., Cardoso, W.V., Varelas, X., 2015. Crumbs3-Mediated Polarity Directs Airway Epithelial Cell Fate through the Hippo Pathway Effector Yap. Dev. Cell 34, 283–296. https://doi.org/10.1016/j.devcel.2015.06.020

Tan, B., Yatim, S.M.J.M., Peng, S., Gunaratne, J., Hunziker, W., Ludwig, A., 2020. The Mammalian Crumbs Complex Defines a Distinct Polarity Domain Apical of Epithelial Tight Junctions. Curr. Biol. CB 30, 2791-2804.e6. https://doi.org/10.1016/j.cub.2020.05.032

Tilston-Lünel, A.M., Haley, K.E., Schlecht, N.F., Wang, Y., Chatterton, A.L.D., Moleirinho, S., Watson, A., Hundal, H.S., Prystowsky, M.B., Gunn-Moore, F.J., Reynolds, P.A., 2016. Crumbs 3b promotes tight junctions in an ezrin-dependent manner in mammalian cells. J. Mol. Cell Biol. 8, 439–455. https://doi.org/10.1093/jmcb/mjw020

Ventura, G., Amiri, A., Thiagarajan, R., Tolonen, M., Doostmohammadi, A., Sedzinski, J., 2022. Multiciliated cells use filopodia to probe tissue mechanics during epithelial integration in vivo. Nat. Commun. 13, 6423. https://doi.org/10.1038/s41467-022-34165-0

Vernale, A., Prünster, M.M., Marchianò, F., Debost, H., Brouilly, N., Rocher, C., Massey-Harroche, D., Renard, E., Le Bivic, A., Habermann, B.H., Borchiellini, C., 2021. Evolution of mechanisms controlling epithelial morphogenesis across animals: new insights from dissociation-reaggregation experiments in the sponge Oscarella lobularis. BMC Ecol. Evol. 21, 160. https://doi.org/10.1186/s12862-021-01866-x

Walentek, P., 2021. Xenopus epidermal and endodermal epithelia as models for mucociliary epithelial evolution, disease, and metaplasia. Genes. N. Y. N 2000 59, e23406. https://doi.org/10.1002/dvg.23406

Walentek, P., Bogusch, S., Thumberger, T., Vick, P., Dubaissi, E., Beyer, T., Blum, M., Schweickert, A., 2014. A novel serotonin-secreting cell type regulates ciliary motility in the mucociliary epidermis of Xenopus tadpoles. Dev. Camb. Engl. 141, 1526–1533. https://doi.org/10.1242/dev.102343

Wang, S., Cha, S.-W., Zorn, A.M., Wylie, C., 2013. Par6b regulates the dynamics of apicobasal polarity during development of the stratified Xenopus epidermis. PloS One 8, e76854. https://doi.org/10.1371/journal.pone.0076854

Wei, Z., Li, Y., Ye, F., Zhang, M., 2015. Structural basis for the phosphorylation-regulated interaction between the cytoplasmic tail of cell polarity protein crumbs and the actin-binding protein moesin. J. Biol. Chem. 290, 11384–11392. https://doi.org/10.1074/jbc.M115.643791

Werner, M.E., Hwang, P., Huisman, F., Taborek, P., Yu, C.C., Mitchell, B.J., 2011. Actin and microtubules drive differential aspects of planar cell polarity in multiciliated cells. J. Cell Biol. 195, 19–26. https://doi.org/10.1083/jcb.201106110

Werner, M.E., Mitchell, B.J., 2012. Understanding ciliated epithelia: the power of Xenopus. Genes. N. Y. N 2000 50, 176–185. https://doi.org/10.1002/dvg.20824

Whiteman, E.L., Fan, S., Harder, J.L., Walton, K.D., Liu, C.-J., Soofi, A., Fogg, V.C., Hershenson, M.B., Dressler, G.R., Deutsch, G.H., Gumucio, D.L., Margolis, B., 2014a. Crumbs3 is essential for proper epithelial development and viability. Mol. Cell. Biol. 34, 43–56. https://doi.org/10.1128/MCB.00999-13

Whiteman, E.L., Fan, S., Harder, J.L., Walton, K.D., Liu, C.-J., Soofi, A., Fogg, V.C., Hershenson, M.B., Dressler, G.R., Deutsch, G.H., Gumucio, D.L., Margolis, B., 2014b. Crumbs3 Is Essential for Proper Epithelial Development and Viability. Mol. Cell. Biol. 34, 43–56. https://doi.org/10.1128/MCB.00999-13

Yasunaga, T., Wiegel, J., Bergen, M.D., Helmstädter, M., Epting, D., Paolini, A., Çiçek, Ö., Radziwill, G., Engel, C., Brox, T., Ronneberger, O., Walentek, P., Ulbrich, M.H., Walz, G., 2022. Microridge-like structures anchor motile cilia. Nat. Commun. 13, 2056. https://doi.org/10.1038/s41467-022-29741-3

Figures

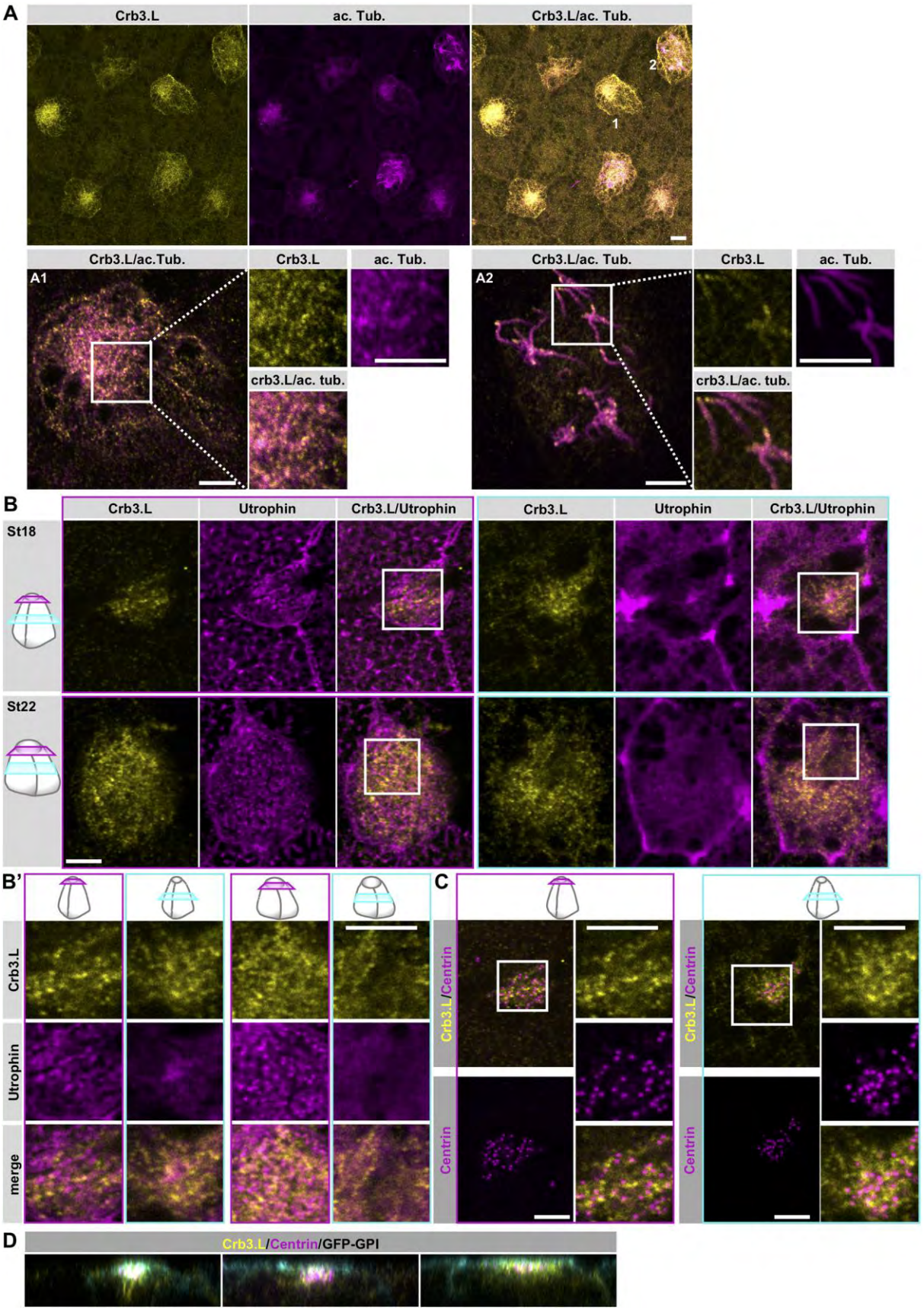

Fig. 1. Crb3.L is expressed in MCCs expanding their apical surface and during ciliogenesis

A-D: Micrographs of MCCs during insertion, expansion of the apical domain and early ciliogenesis in stage 18 embryos.

Crb3.L is labelled with our custom-made anti-Crb3.L. Scale bars are 10 µm.

(A): Crb3.L vesicles are in close association with microtubular tracks in MCCs

Maximal intensity projection of en face view of whole-mount of St 18 *Xenopus laevis* embryos at low magnification. Stable microtubules are labelled with anti-acetylated α-tubulin antibodies (ac. Tub.)

A1, A2: Single confocal section at higher magnification of the MCC 1 and 2 pointed in A. A1 section at the level of the tubulin network in cell 1 sub-apical domain. A2 section at the level of cilia in cell 2. Inserts on the right-side panel A1 and A2 are cropped magnified micrographs of the region of interest (ROI), corresponding to white squares drawn in A1 and A2. Inserts display separate channels and overlay for better appreciation of the localization of Crb3.L regarding stable microtubules. Note the dotty staining of Crb3.L following microtubule tracks in the cytoplasm (A1) and the ciliary axoneme (A2).

(B): Crb3.L vesicles localize within the remodeling actin meshworks in MCCs

F-actin is labelled via injection of *utrophin-gfp* mRNA (Utrophin).

(B): upper row, single x, y confocal sections of an emerging MCC (apical surface 63µm^2) in a stage 18 embryo. Magenta framed panels are at the level of the newly formed apical domain as depicted on the scheme (magenta line indicates the level of the section). Cyan frame panels are at the level of the internal actin meshwork as depicted on the scheme (cyan line indicates the level of the section).

(B) lower row, single x, y confocal sections of a an emerged MCC (apical surface 178 µm^2) in a stage 22 embryo. Magenta framed panels are at the level of the maturing apical actin meshwork as depicted on the scheme (magenta line indicates the level of the section). Cyan frame panels are at the level of the internal actin meshwork as depicted on the scheme (cyan line indicates the level of the section).

(B') cropped magnified micrographs of the ROI, corresponding to white squares drawn in B; cells and levels of section are indicated on the scheme heading each column.

(C): Crb3.L vesicles localize in the vicinity of the ascending centrioles

Centrioles and BBs are labelled by anti-Centrin antibodies.

Single x, y confocal sections of the St18 MCC shown in B. Magenta framed panels are at the level of the centrioles/BBs that have reached the apical domain as depicted on the scheme (magenta line indicates the level of the section). Cyan frame panels are at the level of the internal centrioles/BBs as depicted on the scheme (cyan line indicates the level of the section).

D: Crb3.L localization changes are synchronous to centriole/BB ascension and apical surface emergence in MCCs.

x-z optical sections through a series of MCCs with expanding apical surface. Micrographs are ranked from the smallest (left) to the largest apical cell surface. Note the progressive shift of Crb3.L from an internal position when centrioles/BBs are deep in the cytoplasm to the apical domain when BBs are docked at the apical surface.

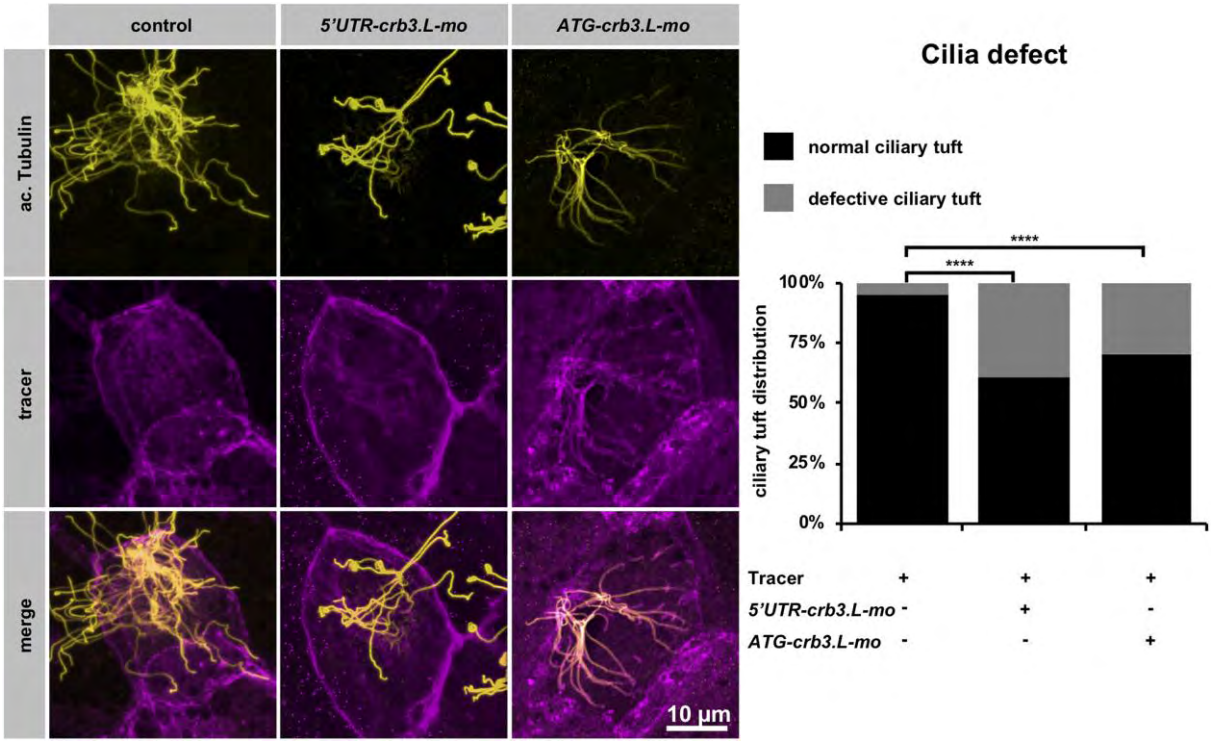

Fig. 2. Crb3.L is required for ciliogenesis in MCCs

A: En face view of stage 28 embryos, control embryos are injected with 200 pg of *m-RFP* mRNA, morphants are co-injected with 200 pg of *m-RFP* mRNA and either 15 ng of 5'UTR targeting morpholino (*5'UTR-crb3.L-mo*) or 30 ng of ATG targeting morpholino (*ATG-crb3.L-mo*) and *mRFP* mRNA. Cilia are labeled with anti-acetylated α-Tubulin.

B: Bar charts showing the quantification of the cilia defects. For quantification, the value 1 was assigned to well-furnished cilia tufts as in control cells (see anti-acetylated α-Tubulin control picture, the value 0 was assigned to defective cilia tuft displaying an obviously low cilia number and/or very short cilia such as in morphant cells (see anti acetylated α-Tubulin in morphants). χ^2test, followed by pairwise comparison using Bonferroni correction. Controls (8 embryos, 94 MCCs), *5'UTR-crb3.L-mo* (8 embryos, 56 MCCs), *ATG-crb3.L-mo* (20 embryos; 225 MCCs). ****p<0,001. Pictures and bar charts from one representative experiment out of 3 experiments.

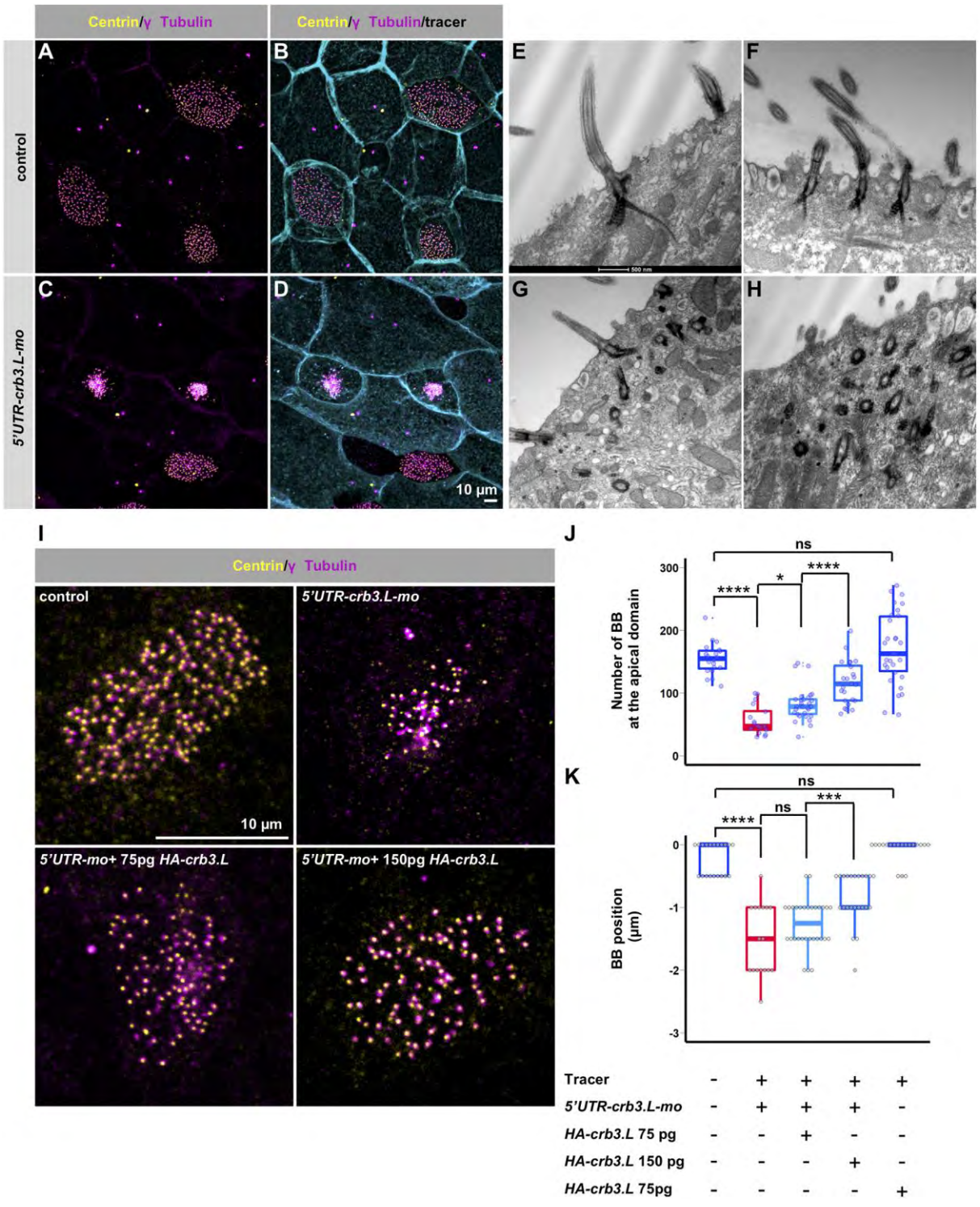

Fig. 3. crb3.L is required for proper BB migration and docking

(A-D): Maximum intensity projection of en face view stage 28 embryos. BBs are labeled with anti-Centrin (centriole) and anti γ-Tubulin (basal foot) antibodies.

Control embryos are injected with 200 pg of *GFP-GPI* mRNA, morphants are co-injected with 200 pg of *GFP-GPI* mRNA and 15 ng of *5'UTR-crb3.L-mo*.

(E-H) TEM picture of the skin of stage 28 embryos. (E, F) control embryos, (G, H) morphant embryos.

Note the even distribution of BBs covering most of the apical surface in control embryos (A, B, F, I) whereas in morphant embryos apically located BBs occupy a restricted part of the cell surface, are clumped together and stay deep in the cytoplasm (C, G, H)

(I-J) Rescue experiment showing correction of the BB migration/docking defect with morpholino insensitive HA tagged *crb3.L mRNA.*

(I) Most apical slice of a representative MCC, in the 4 following injection conditions: control (no injection), co injection of 15 ng *5'UTR-crb3.L-mo* and tracer, co injection of 15 ng *5'UTR-crb3.L-mo* and 75 pg *HA-crb3.L* mRNA and tracer, co injection of 15 ng *5'UTR-crb3.L-mo* and 150 pg *HA-crb3.L* mRNA and tracer.

(J, K) To assess the rescue, we estimated two parameters: the number of BBs docked on the apical surface (upper graph J) and the position of the BBs relative to the cell apical surface (lower graph K). Injection conditions are common to the two graphs, and are depicted below the BBs position graph. mo refers to *5'UTR-crb3L-mo.*

(J)The number of apically located BBs was automatically counted with the find maxima tool of the Fiji software.

(K) To estimate BB position relative to the apical cell surface, the number of planes occupied by at least 3 BBs were counted. Noninjected control (n=20), co injection 15 ng of *5'UTR-crb3L-mo* and tracer (n=19), co injection of 15 ng *5'UTR-crb3L-mo* and 75 pg *HA-crb3.L* mRNA and tracer (n=24), co injection of 15 ng *5'UTR-crb3L-mo* and 150 pg *HA-crb3.L* mRNA and tracer (n=32), 75 pg *HA-crb3.L* mRNA (n=21), n= number of cells.

Results are presented with Box-plots, box displays the interquartile range (50% of the distribution) and whiskers highlight 1,5 interquartile range, median is shown. *p<0,05, ***p<0,005, ****p<0,001

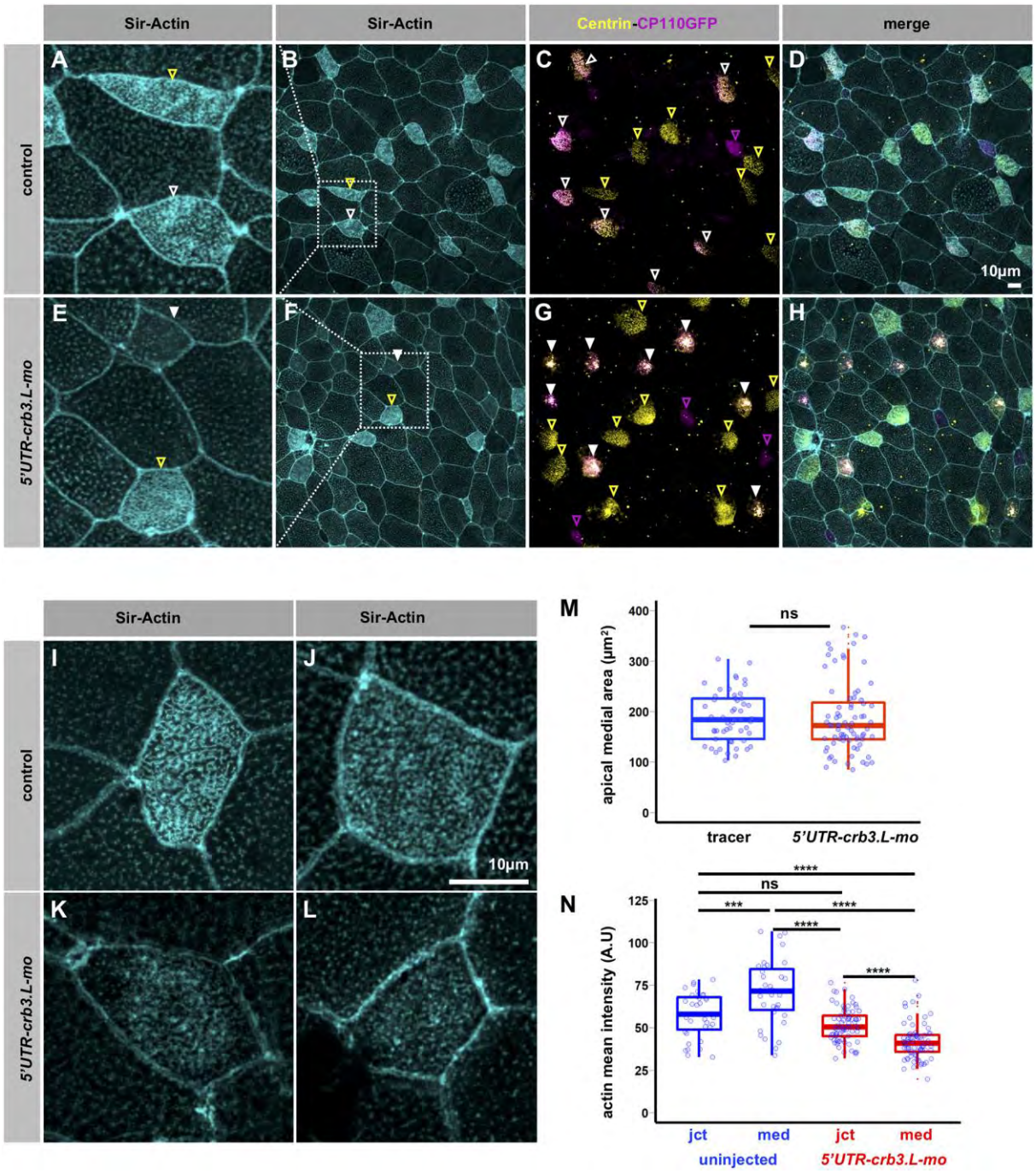

Fig. 4. Crb3.L is required for proper organization of the actin cytoskeleton in MCCs

(A-H) Maximum intensity projection of whole-mount stage 28 embryos, actin is stained with the Sir-actin probe, BBs are detected with anti-Centrin antibodies, *cp110-GFP* mRNA is a tracer labelling BBs in injected cells. (A-D) Mosaic control injected with *cp110-GFP* mRNA, (I-H) mosaic morphants co-injected with *5'UTR-crb3L-mo* and *cp110-GFP* mRNA. (C, G) Noninjected MCCs are detected via Centrin endogenous staining displayed in the yellow channel in both mosaic controls and morphants (yellow contoured arrowheads). Non-MCCs cells are labelled with Cp110-gfp displayed in the magenta channel (magenta contoured arrowheads). Injected MCCs are revealed by doubly labelled

BBs (endogenous Centrin+ injected *cp110-GFP* tracer) and thus appear in a orange-pink to white range of color. White contoured arrowheads point to control tracer injected MCCs. White filled arrowheads point to (*5'UTR-crb3L-mo* + *cp110-GFP* tracer) injected MCCs. BB intracytoplasmic aggregation results in a bright orange-pink to white signal (white filled arrow).

(A-E) crop image of the ROI delineated by the white dashed square in B and F.

(I-L) Higher magnification of the actin meshwork in control and morphant MCCs.

(M) Measures of apical medial area in control tracer injected embryos (tracer) and *5'UTR-crb3.L* morphants (5'UTR-crb3.L-mo). The apical medial area delimited by the apical cell-cell junction, is a proxi for the apical cell surface.

(N) Quantification of the actin cytoskeleton defect, junctional (**jct**) and medial (**med**) actin mean intensity are measured in the MCCs of mosaic *5'UTR-crb3.L* morphants. Absence of variation in junctional actin intensity between noninjected and *5'UTR-crb3.L* injected MCCs, enable interpretation of variation of medial actin intensity. Mean actin intensity is presented in arbitrary unit. (Mosaic morphants embryos n=7, noninjected cells n=35, morpholino injected cell n=72.Pictures and graphs from one representative experiment out of 3 experiments.

Results are presented with Box-plots, box displays the interquartile range (50% of the distribution) and whiskers highlight 1,5 interquartile range, median is shown. ***p<0,005, ****p<0,001

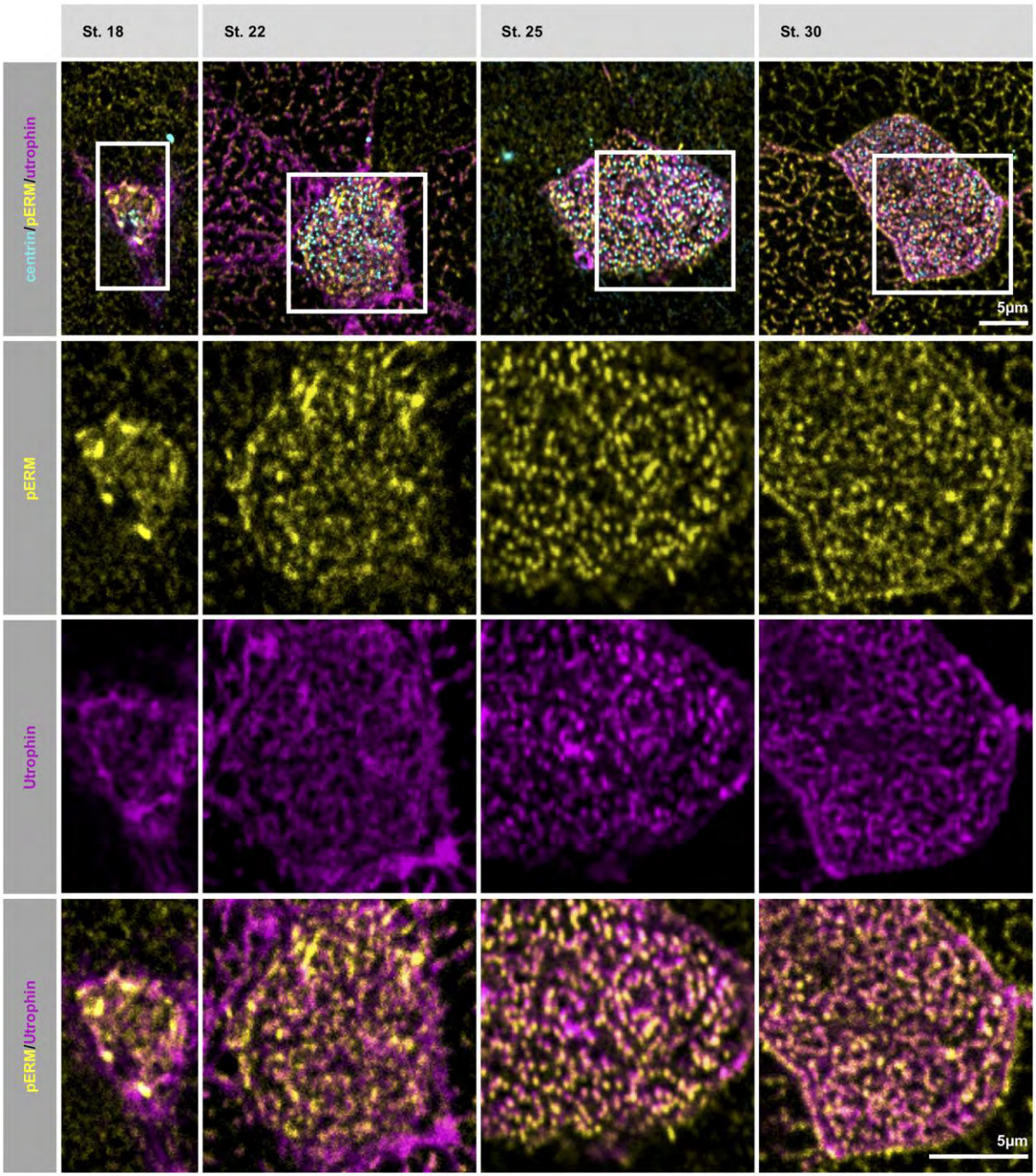

Fig. 5. Endogenous pERM expression in MCCs

Single confocal section of whole-mount embryos between stages 18 and 30, focusing on the emerging and maturing apical domain of MCCs. pERM detection is coupled Utrophin-GFP to label actin. BBs are detected with anti-Centrin antibodies. ROIs are shown by white squares in the first row, cropped magnified pictures corresponding to these ROIs are presented in the following rows.

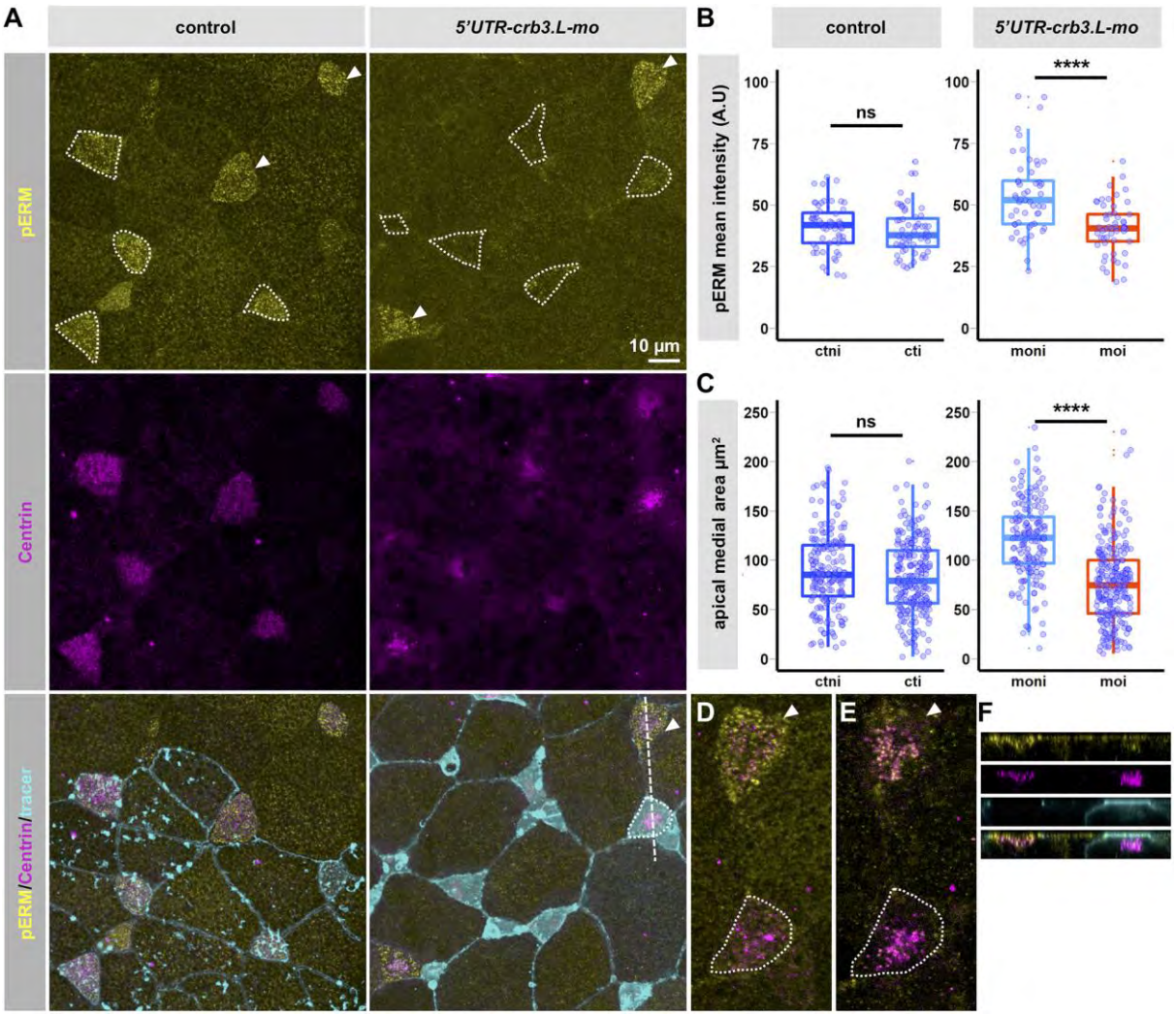

Fig. 6. Crb3.L regulates pERM at the developing apical surface of MCCs and is important for apical surface expansion

(A) Maximum intensity projection of a whole-mount mosaic tracer injected control and *5'UTR-crb3.L* morphant stained with anti-pERM antibodies. BBs are detected with anti-Centrin antibodies, GFP-GPI is the tracer for injected cells in control and morphant stage 21 embryos. Tracer Injected, or tracer + morpholino injected MCCs are encircled by dotted lines. Noninjected MCCs are indicated by white arrowheads.

(B) Quantification of pERM intensity in mosaic control and 5'UTR-crb3L morphants. To avoid inter- and intra-embryos non-biological staining variations, only mosaic injected regions were considered for quantification in control and *5'UTR-crb3.L* morphants at stage 21. Mosaic frames containing more than 2 injected and 2 noninjected MCCs were used for quantification to allow calculation of the average intensity of pERM staining in each cell population per frame. Absence of variation of the staining in mosaic controls was a prerequisite for considering a variation observed in mosaic morphant as significant. Box plots present the average intensity of pERM staining per frame in MCCs

of mosaic controls (left) and mosaic morphants (right). noninjected control MCCs (**ctni**), tracer injected MCCs (**cti**) MCCs, noninjected morphant MCCs (**moni**), *5'UTR-crb3L*-morpholino + tracer injected MCCs (**moi**). Pictures and graphs from one representative experiment out of 3 experiments. Mosaic controls (n=9, 187 noninjected cells and 246 injected cells, 56 frames), mosaic morphants (n=9, 176 noninjected cells and 268 injected cells, 53 frames).

(C) Quantification of the size of the apical domain in mosaic control and *5'UTR-crb3L* morphants at stage 21. Measures are performed on the pictures selected for figure 6B. Absence of variation in the apical surface in mosaic controls was a prerequisite for considering a variation observed in mosaic morphant as significant. Box plots present the distribution of the individual measures of apical surface in MCCs of mosaic controls (left) and mosaic morphants (right). noninjected control MCCs (**ctni**), tracer injected MCCs (**cti**) MCCs, noninjected morphant MCCs (**moni**), 5'UTR-crb3L-morpholino + tracer injected MCCs (**moi**). Pictures and graphs from one representative experiment out of 3 experiments. Mosaic controls (n=9, 187 noninjected cells and 246 injected cells, 56 frames), mosaic morphants (n=9, 176 noninjected cells and 268 injected cells, 53 frames).

(D-F) pERM recruitement at BBs in a mosaic morphant embryo

(D, E) higher magnification of single focal plane at the level of the apical surface (D), and inside the cells at the level of ascending BBs (E). The noninjected cell is pointed by the white arrowhead, the injected cell is surrounded by the red dotted line.

(F):x,z optical section according to dotted line in A, channel color code is the same as in A. Note that this configuration (noninjected and injected cells with similar apical surface and ascending BBs) is an extremely rare event making difficult quantification of pERM at BBs.

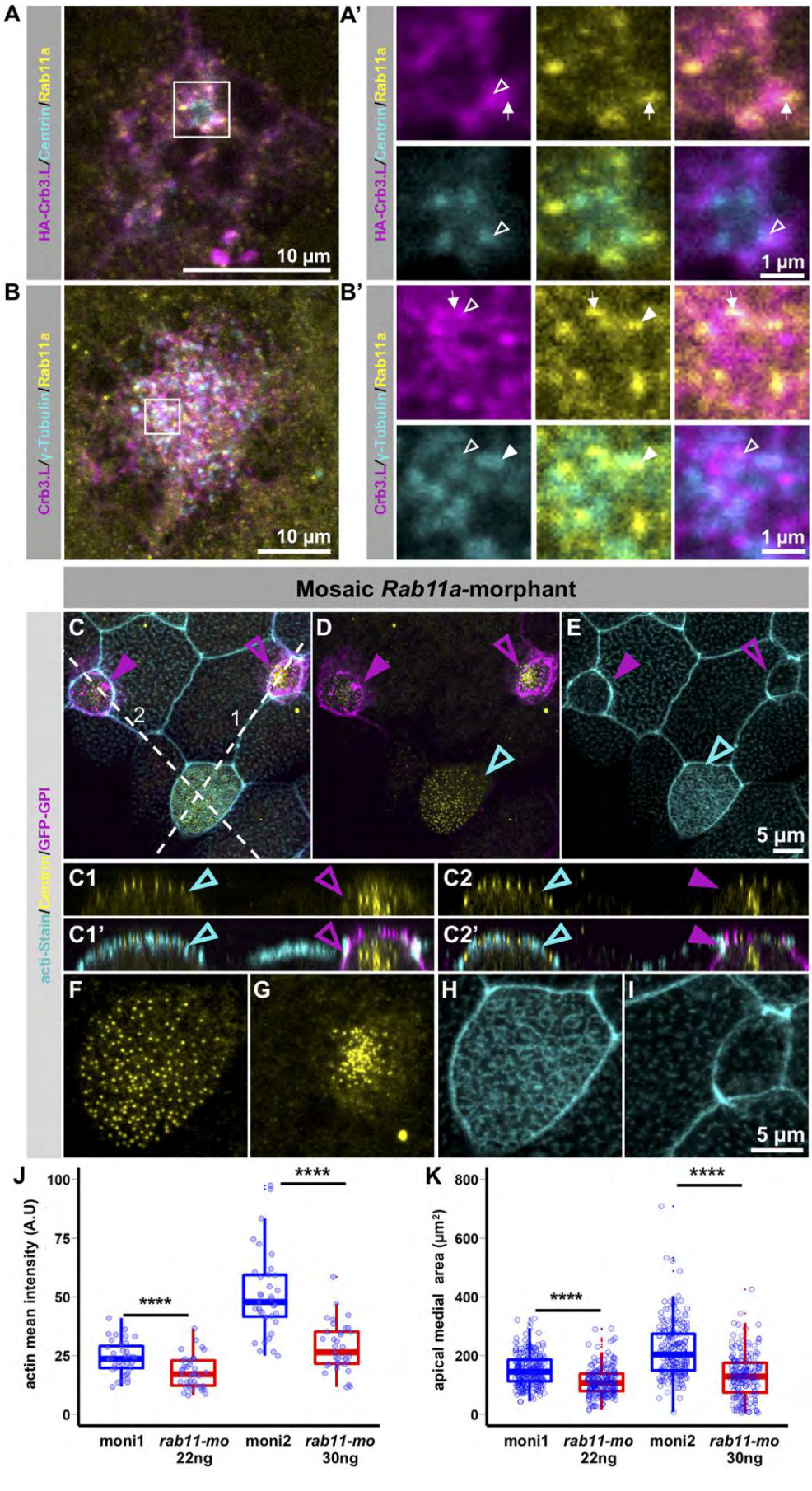

Fig. 7. Crb3.L and Rab11 might cooperate for centrioles/BBs ascension

(A) single confocal section of an inserting MCC in a stage 20 embryo co-injected with *centrin-RFP* mRNA to label centrioles/BBs, and *HA-crb3.L*. HA-Crb3.L and endogenous Rab11a are detected with anti HA and anti Rab11a respectively.

(A'): 6 cropped magnified micrographs of the region of interest (ROI) corresponding to the white square drawn in A. These inserts display separate channels and overlay for better appreciation of the localization of HA-Crb3.L regarding Rab11a vesicles and centrioles/BBs.

(B) single confocal section of an emerging MCC in a stage 20 wild type embryo. BBs, endogenous Crb3.L, and endogenous Rab11a are respectively labelled with anti γ-Tubulin, anti Crb3.L and anti Rab11a antibodies.

(B') 6 cropped magnified micrographs of the region of interest (ROI) corresponding to the white square drawn in B. Note the partial overlap of Rab11 with Crb3.L (white arrows), the partial overlap of Rab11a and γ-Tubulin or Centrin (white arrowheads) and the partial overlap of Crb3.L and Centrin (white contoured arrowheads).

(C-E) Maximum intensity projection of a whole-mount mosaic *rab11*-morphant. BBs are detected with anti-Centrin antibodies, F-actin is stained with the Acti Stain™ probe, GFP-GPI is the tracer for injected cells. The noninjected MCC is indicated by a cyan contoured arrowhead whereas the two *rab11a*-morpholino injected cells are indicated by magenta arrowheads. Filled and contoured magenta arrowheads are used to distinguished the two Rab11a depleted cells on x, z optical confocal sections corresponding to the axis 1 and 2 drown in (C).

(D, C1-C2 ,F,G) displays the centrioles/BBs phenotype. F and G are cropped magnified micrographies of D. (F) noninjected control MCC, (G) *rab11a*-morpholino injected MCC pointed by the countered magenta arrowhead.

(H, I) Higher magnification of the actin meshwork. (H), noninjected control MCC, (I) *rab11a*-morpholino injected MCC pointed by the countered magenta arrowhead.

(J, K) Quantification of the actin cytoskeleton and apical medial area in mosaic *rab11a*-morphants. Graphs present the results of 2 independent experiments performed with two *rab11a*-morpholino doses, experiment 1 with 22ng, experiment 2 with 30 ng per blastomere. Measures were performed in control tracer injected mosaic embryos and mosaic *rab11*a-morphants in stage 22 embryos. Absence of variation actin density and apical surface between noninjected and tracer injected cells was verified in control but is not presented on the graphs *(experiment 1 ct=7 noninjected cells 193, injected cells 187, number of frame 33, morphants n=8, noninjected cells 259, injected cells 201, number of frame 37, experiment 2 ct=4 noninjected cells n=75, injected cells n=79, number of frame 13, morphants n=8, noninjected cells 191, injected cells 177, number of frame 35).* Experiment 1: Noninjected morphant MCCs

(**moni1**), *rab11a*-morpholino + tracer injected MCCs (**mo 22 ng).** Experiment 2: noninjected morphant MCCs (**moni2**), *rab11a*-morpholino + tracer injected MCCs experiment 2 (**mo 30 ng).**

(J) Quantification of the actin cytoskeleton defect, medial regions were manually delineated excluding the junctions, mean actin intensity was measured with Fiji and is presented in arbitrary unit.

(K) Quantification of the apical medial area. The apical medial area delimited by the apical cell-cell junction, is a proxi for the apical cell surface.

Results are presented with Box-plots, box displays the interquartile range (50% of the distribution) and whiskers highlight 1,5 interquartile range, median is shown. ****p<0,001.

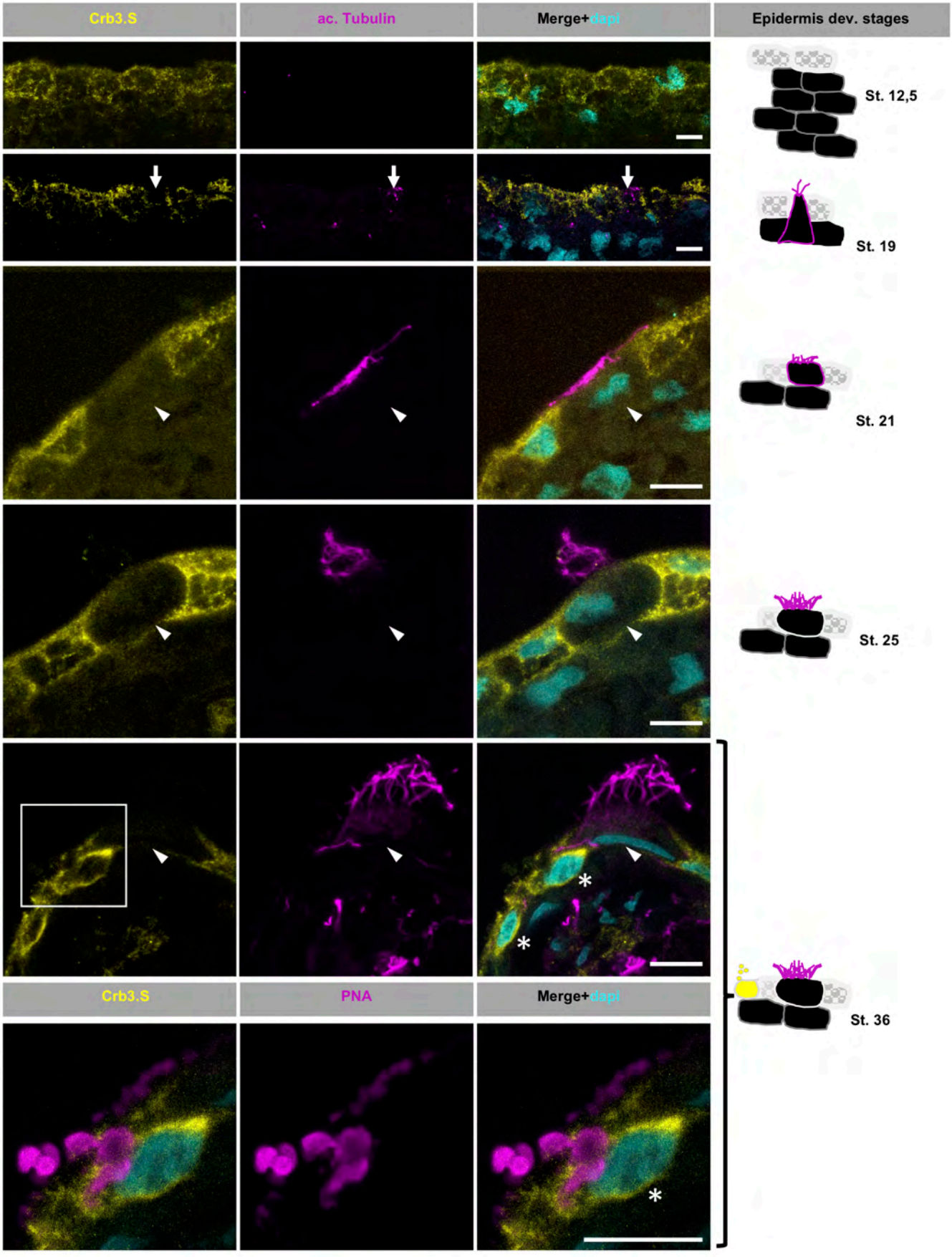

Supplementary figure 1

Fig. S1. Crb3.S has an early, dynamic, and wide expression during morphogenesis of the mucociliary epidermis

A : Frozen sections displaying Crb3.S custom-made antibody staining during morphogenesis of the mucociliary epidermis. Schemes on the right depict *Xenopus* epidermis morphogenetic changes according to the developmental stages. Nuclear staining is DAPI, cilia are labelled with anti-acetylated α-Tubulin (ac-Tubulin), peanut agglutin (PNA) stains small and large secretory vesicles of goblet cells and SSCs, respectively. (white arrows) newly formed cilia, (white arrowheads): MCC, (stars): SSC. Scale bars are 10 µm.

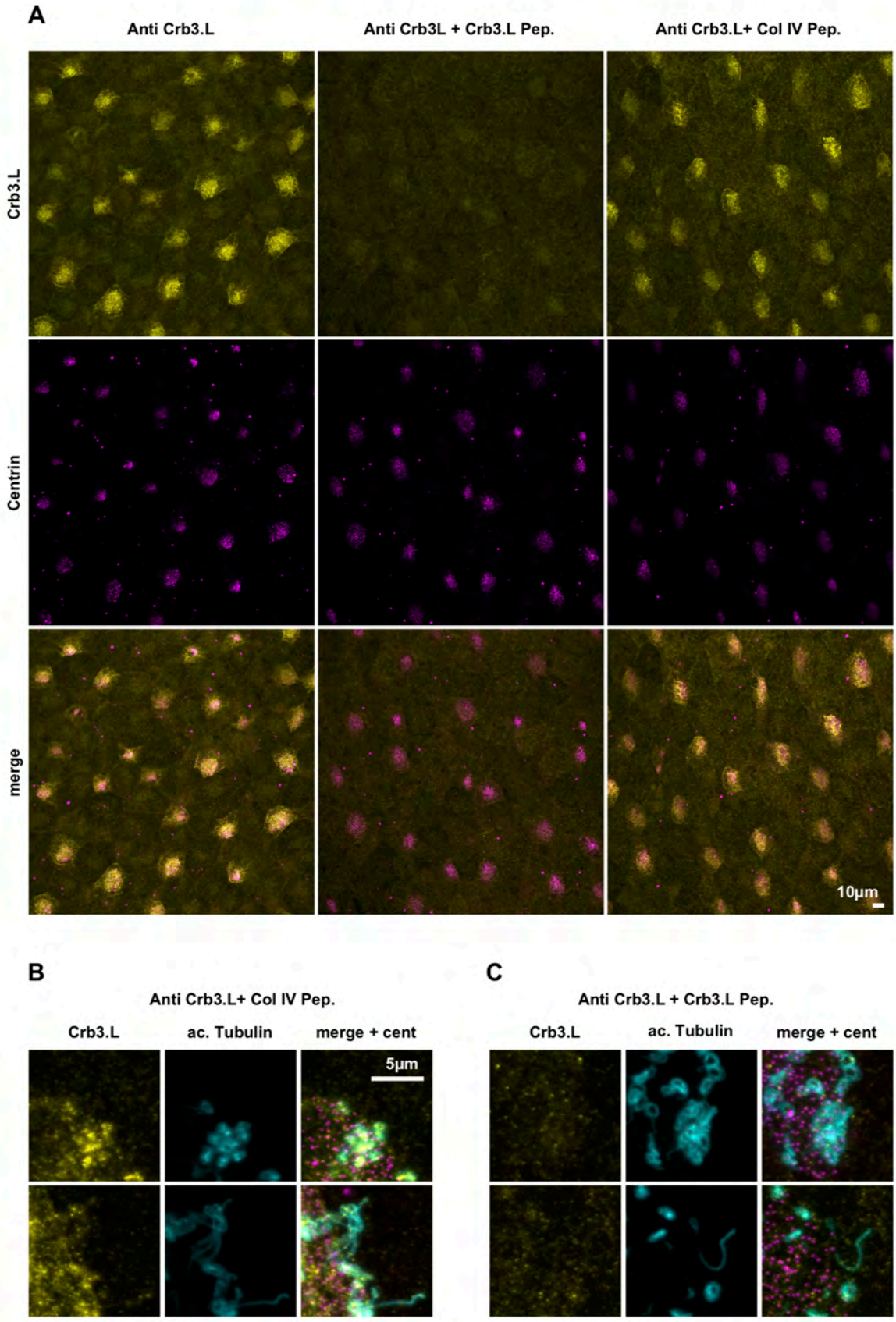

Supplementary figure 2a

Fig. 2a. Crb3.L antibody staining is lost in immunogenic peptide competition assay A-C: Maximal intensity projection of whole-mount St 20-21 *Xenopus laevis* embryonic mucociliary epidermis stained with anti Crb3.L antibody in control condition, in competitive condition with the addition of the immunogenic peptide, in control condition with the addition of an unrelated peptide (*Oopsacas. minuta* type IV collagen). The ratio between antibody and peptides was 1 to 25 moles. BBs were labelled with anti-Centrin antibody. Crb3.L staining in MCCs is efficiently decreased upon competition with the immunogenic peptide.

B-C: Higher magnification focusing on cilia. Cilia were labelled with anti-acetylated α-Tubulin antibody. Note Crb3.L spotted staining on cilia when the Crb3.L antibody is preincubated with a none-related peptide. C: Note the disappearance of the ciliary signal upon immunogenic peptide competition.

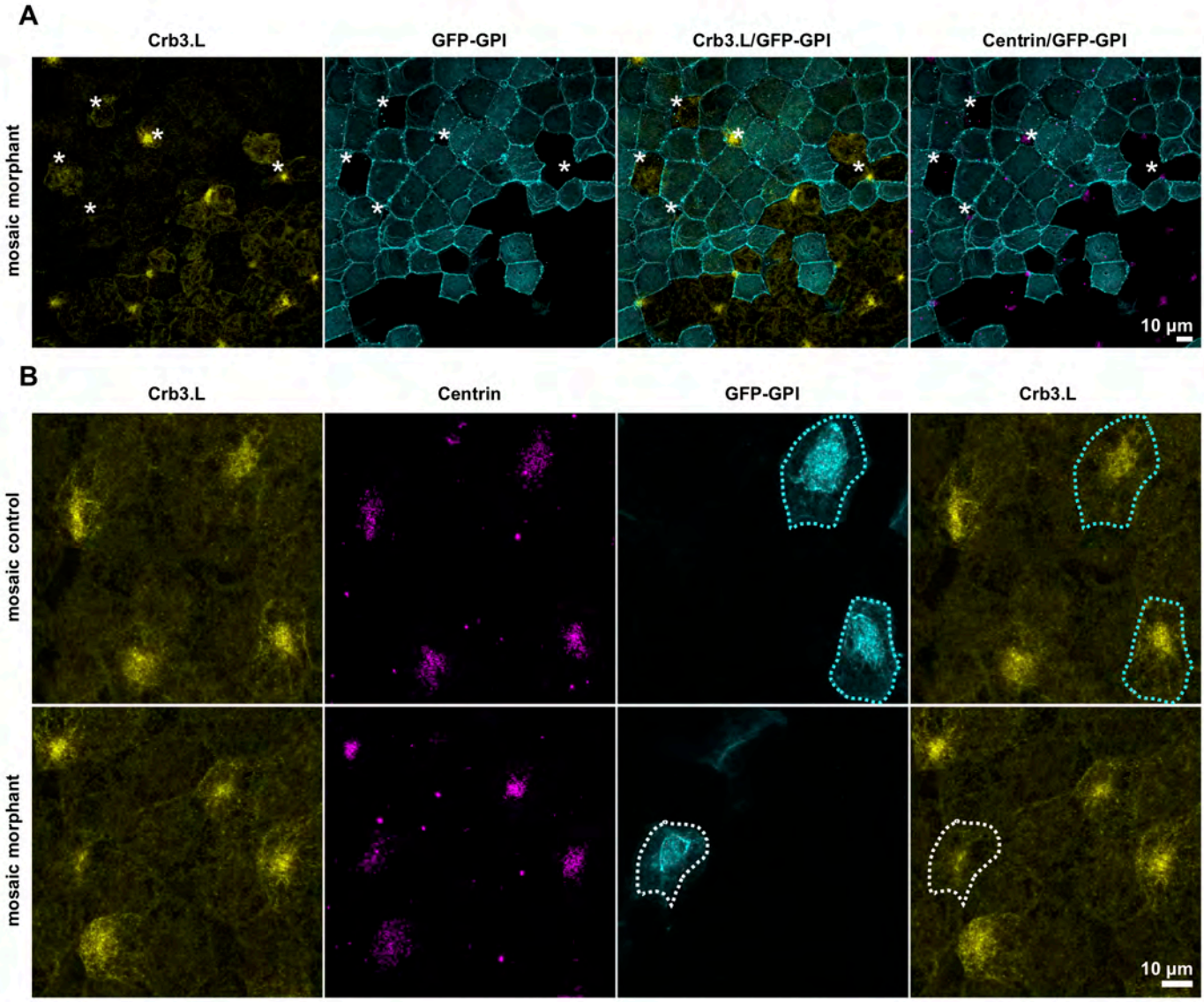

Supplementary figure 2b

Fig. 2b. Crb3.L antibody staining decreases upon *crb3.L* morpholino depletion A-B: Maximal intensity projection of whole-mount St 20 *Xenopus laevis* embryos. Control embryos were injected with 200 pg *GFP-GPI* mRNA to label cell membranes. Morphants were injected with *GFP- GPI* mRNA and anti *crb3.L* morpholino. Mosaic regions of control and morphant embryos allow easy comparison of Crb3.L staining between noninjected and tracer injected cells (in control embryo), or noninjected and Crb3.L-depleted cells (in morphants). BBs are detected with anti-Centrin antibody, cell membranes are labelled with GFP-GPI.

A: mosaic morphant region showing that Crb3.L expression is globally decreased in all injected cells, including non-MCCs cells. *indicates noninjected cells or area in otherwise *5'UTR-crb3.L-mo* injected region B: mosaic regions focusing on MCCs expanding their apical surface. White dotted lines surround *crb3.L* morpholino and tracer injected MCCs. Cyan dotted lines surround control MCCs injected with the tracer alone.

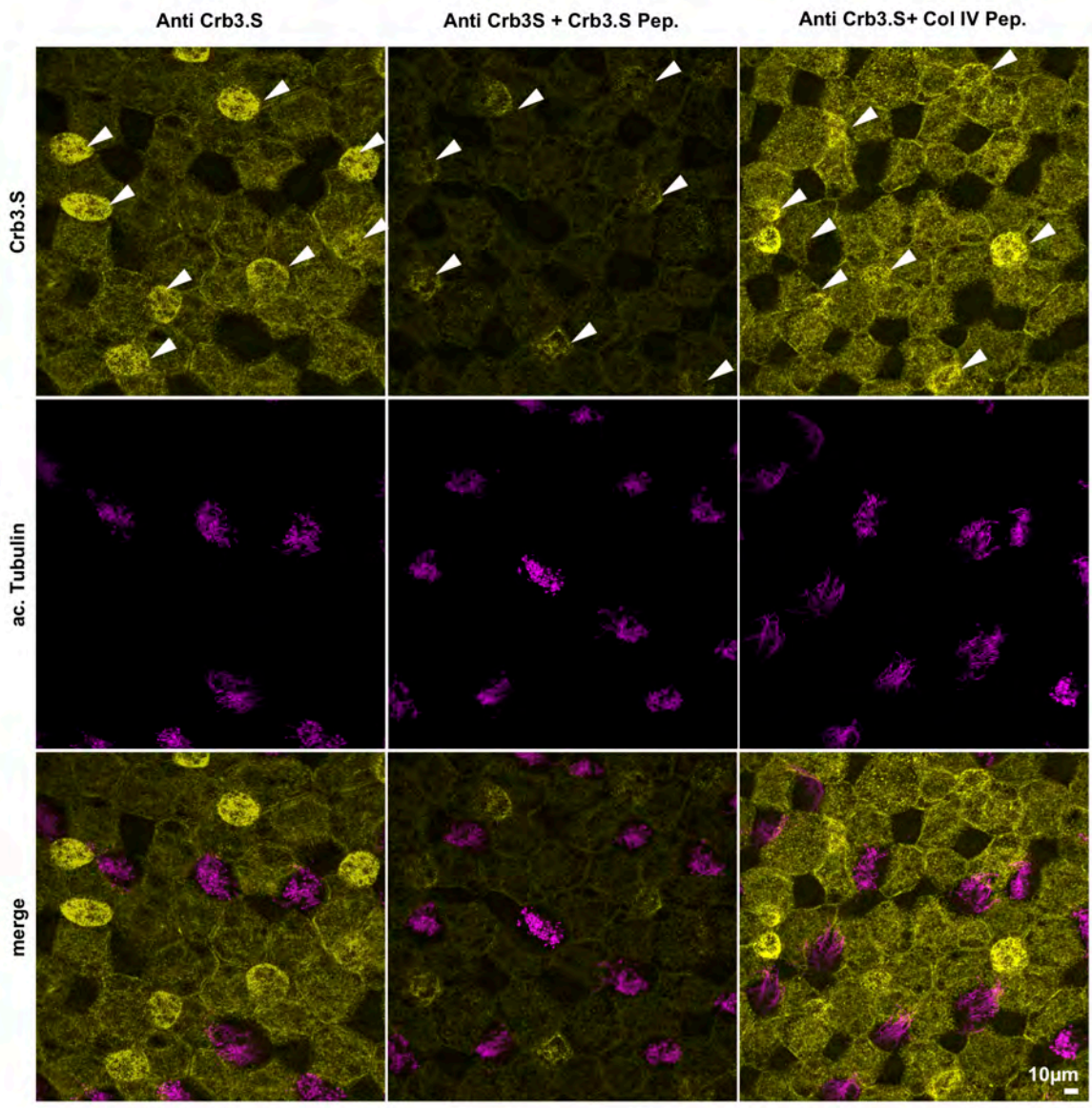

Supplementary figure 3

Fig. S3. Crb3.S antibody staining decreases in immunogenic peptide competition assay

Pictures are maximal intensity projection of en face view of whole-mount St 32 heterozygous *Xenopus laevis albino* embryos stained with Crb3.S, in control condition, in competitive condition with the addition of the immunogenic peptide, in control condition with the addition of an unrelated peptide (*Oopsacas. minuta* type IV collagen). The ratio between antibody and peptides was 1 to 25 moles. White arrowheads point at SSCs, which express the highest level of Crb3.S, as revealed in supplementary figure 1. Note the drastic diminution of Crb3.S staining in the SSCs upon immunogenic peptide incubation.

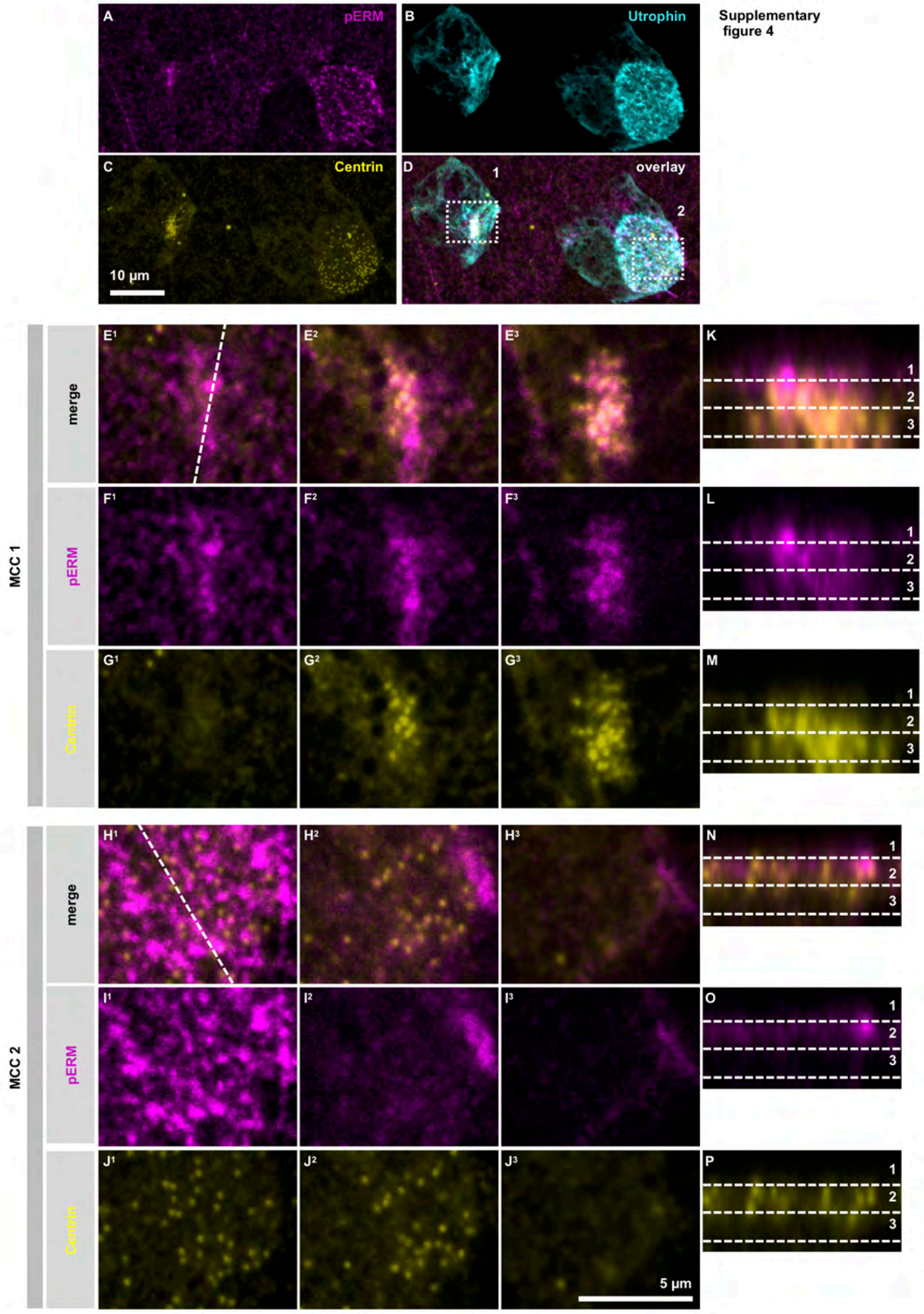

Supplementary figure 4

Fig. S4. pERM is transiently recruited at BBs during their ascension.

(A-D) Maximum intensity projection of early inserting MCCs in stage 18 embryos. Embryos were injected with *utrophin-gfp* mRNA to label actin, stained with anti-Centrin to label centrioles/ BBs, and anti-pERM. (D) MCC 1 is just pointing at the apical surface, MCC 2 is well engaged in apical surface expansion (135 μm^2). The white dotted rectangles delimit the cropped regions of MCC 1 and MCC 2 that are used for examination of p-ERM staining at different cell levels in panels (E^1-P).

(E^1-J^3) confocal x, y planes of the apical surfaces and two intracytoplasmic x, y sections of increasing depth are presented for MCC 1 and MCC 2. (E^1, F^1, G^1, H^1, I^1, J^1) are the most apical planes.

(K-P) are x, z optical confocal sections of MCC 1 and MCC 2.

(E^1-P) Precise coordinates of each confocal sections are explained below.

In E^1 the dotted line indicates the x, z axis for the optical sections presented in K, L, M.

In H^1 the dotted line indicates the x, z axis for the optical sections presented in N, O, P.

The dotted lines (1, 2, 3) in (K-P) indicate the level of the x, y sections presented in (E^1-J^3).

Table S1. primary antibodies

Primary antibodies	Specie/isotype	reference	Dilution	fixation
Ezrin (phospho T567)	Rabbit polyclonal	# 47293 abcam	1/200	PFA 4% 1h RT
γ-Tubulin	mouse IgG1	ref T5326 Sigma-Aldrich	1/800	
Rab11a	mouse IgG2a	ref 610656 BD corresponding to XB 17328586 in Xenbase	1/200	
Crb3.S	rabbit polyclonal	This work	1/200	MEMFA 2h RT followed by 100% methanol at -20°c
Crb3.L	rabbit polyclonal	This work	1/200	
Centrin	mouse IgG2	ref 04-1624-Merck-Millipore	1/1000t	PFA 4% 1h RT Or MEMFA 2h RT followed by 100% methanol at -20°c
α-acetylated Tubulin	mouse IgG2b	T6793 Sigma-Aldrich	1/500	
RFP	rat IgG2a	5F8 Chromotek	1/500	
GFP	chicken polyclonal	GFP-1020 AvesLab	1/500	
HA	mouse IgG1	# 49969 Abcam	1/500	

Table S2. Secondary antibodies

Secondary antibodies alexa fluor	reference	dilution
anti mouse IgG-488	A-11029 Life technologies	1/500
anti mouse IgG- 546	A-11003 Life technologies	
anti mouse IgG- 647	A-21235 Life technologies	
anti mouse IgG1- 647	A-21240 Life technologies	
anti mouse IgG2a-647	A-21241 Life technologies	
anti-mouse IgG2a-488	A-21131 Life technologies	
anti mouse IgG2b-647	A-21242 Life technologies	
anti rat IgG(H+L)-568	A-11077 Life technologies	
anti rabbit IgG-488	A-11008 Life technologies	
anti rabbit IgG-546	A-11035Life technologies	
anti chicken IgY-488	A11039 Life technologies	

Table S3. Fluorescent probes

probes	reference	dilution	fixation
SiR-actin	Spirochrome SC001	1/1000	PFA 4% 1h RT
Acti stain 670	Cytoskeleton, Inc.	1/150-	
PNA FITC-conjugated	L7381 Sigma Aldrich	1/10000	MEMFA 2h RT followed by 100% methanol at -20°c